Multiwavelength Monitoring of the BL Lacertae Object PKS 2155-304 in May 1994. II. The IUE Campaign

Elena Pian[1,2], C. Megan Urry[1,2], Aldo Treves[3,4], Laura Maraschi[5,2],

Steve Penton[6], J. Michael Shull[6], Joseph E. Pesce[1,2], Paola Grandi[7],

Tsuneo Kii[8], Ron I. Kollgaard[9], Greg Madejski[10], Herman Marshall[11],

Willem Wamsteker[12], Annalisa Celotti[4,13], Thierry J.-L. Courvoisier[14],

Renato Falomo[15], Henner H. Fink[16], Ian M. George[10], Gabriele Ghisellini[17]

Received _____; accepted _____

[1]Space Telescope Science Institute, 3700 San Martin Drive, Baltimore, MD 21218

[2]Guest Observer with the International Ultraviolet Explorer

[3]Dpt. of Physics, University of Milan, via Celoria 16, I-20133 Milan, Italy

[4]Scuola Internazionale Superiore di Studi Avanzati, via Beirut 2-4, I-34014 Trieste, Italy

[5]Osservatorio Astronomico di Brera, via Brera 28, I-20121 Milano, Italy

[6]University of Colorado, JILA, Campus Box 440, Boulder, CO 80309-0440

[7]IAS/CNR, via Enrico Fermi 23, CP67, I-00044 Frascati, Italy

[8]Institute for Space and Astronautical Science, 3-1-1 Yoshinodai, Sagamihara, Kanagawa 229, Japan

[9]Department of Astronomy and Astrophysics, The Pennsylvania State University, University Park, PA 16802

[10]Laboratory for High Energy Astrophysics, Goddard Space Flight Center, Greenbelt, MD 20771

[11]Eureka Scientific, Inc., 2452 Delmer St., Suite 100, Oakland, CA 94602

[12]ESA IUE Observatory, P.O. Box 50727, 28080 Madrid, Spain

[13]Institute of Astronomy, Madingley Road, Cambridge, CB3 0HA, United Kingdom

[14]INTEGRAL Science Data Centre, 16 Chemin d'Ecogia, CH-1290 Versoix, Switzerland

[15]Osservatorio Astronomico di Padova, via dell'Osservatorio 5, I-35122 Padova, Italy

[16]Max Planck-Institute für Extraterrestrische Physik, Giessenbachstrasse, 85740 Garching bei München, Germany

[17]Osservatorio Astronomico di Brera, via Bianchi 46, I-22055 Merate, Italy

ABSTRACT

PKS 2155-304, the brightest BL Lac object in the ultraviolet sky, was monitored with the IUE satellite at ∼1 hour time-resolution for ten nearly uninterrupted days in May 1994. The campaign, which was coordinated with EUVE, ROSAT, and ASCA monitoring, along with optical and radio observations from the ground, yielded the largest set of spectra and the richest short time scale variability information ever gathered for a blazar at UV wavelengths. The source flared dramatically during the first day, with an increase by a factor ∼2.2 in an hour and a half. In subsequent days, the flux maintained a nearly constant level for ∼5 days, then flared with ∼35% amplitude for two days. The same variability was seen in both short- and long-wavelength IUE light curves, with zero formal lag ($\lesssim$ 2 hr), except during the rapid initial flare, when the variations were not resolved. Spectral index variations were small and not clearly correlated with flux. The flux variability observed in the present monitoring is so rapid that for the first time, based on the UV emission alone, the traditional $\Delta L/\Delta t$ limit indicating relativistic beaming is exceeded. The most rapid variations, under the likely assumption of synchrotron radiation, lead to a lower limit of 1 G on the magnetic field strength in the UV emitting region. These results are compared with earlier intensive monitoring of PKS 2155–304 with IUE in November 1991, when the UV flux variations had completely different characteristics.

Subject headings: galaxies: active — galaxies: BL Lacertae objects: individual (PKS 2155–304) — ultraviolet: galaxies — ultraviolet: spectra

1. Introduction

Variability of active galactic nuclei (AGN) provides the clearest evidence for dynamic processes occurring in the central engines and in the jets of these objects. Its study is therefore a powerful way to investigate the innermost regions of AGN and the emission mechanisms responsible for the huge observed luminosities.

The emission from blazars spans the range from radio to γ-ray energies, and exhibits more rapid and higher amplitude variability than other AGN (Bregman 1990; Wagner & Witzel 1995). Therefore, simultaneous multiwavelength monitoring of blazars is particularly suited to estimating the sizes of the emitting regions (as a function of wavelength) and to understanding, through correlated variability at different frequencies, the radiation processes.

The most widely accepted picture for blazar emission at radio through UV wavelengths is the synchrotron process within an inhomogeneous jet. The model is typically characterized by a spatial dependence of the magnetic field, electron density and maximum electron energy, and usually incorporates a relativistic velocity of the plasma within the jet, which causes beaming of the radiation. How the power is transported along the jet and transferred to the high energy electrons responsible for the observed emission is still unknown. Particle acceleration may take place at a single (dominant) shock front or in a quasi-continuous way (small shocks) along the jet. In the former case, the spectral energy distribution from the millimeter to the soft X-rays derives from the energy distribution of the relativistic electrons accelerated at the shock front, with lower energy particles extending farther from the shock due to their longer lifetimes. In the case of *in situ* acceleration (Marscher 1980; Königl 1981; Ghisellini, Maraschi, & Treves 1985; Hutter & Mufson 1986) the maximum emitted synchrotron frequency usually decreases along the jet, with UV and soft X-rays being produced closest to the central active source.

In PKS 2155–304, the brightest known BL Lac object at UV wavelengths, synchrotron emission produces the optical and UV continuum, as demonstrated by simultaneous spectropolarimetric observations in the two bands (Allen et al. 1993). The synchrotron emission extends to the medium X-ray range (Kii et al. 1996) and has a maximum power per decade (νF_ν) between the UV and soft X-ray range (Wandel & Urry 1991). The spectral steepening from optical to UV to X-rays can be attributed to radiative energy losses in the single shock model, or to the decreasing volume of the region emitting at higher frequencies in the inhomogeneous jet model. In either case the highest amplitude synchrotron variability is expected to be observed at or above the peak power output, which is determined by the steady-state balance of electron acceleration and radiation, since small changes in the electron acceleration substantially alter the higher energy emission.

Previous monitoring of PKS 2155–304 with IUE probed its variability in the far-UV domain (1200-3000 Å) on a range of time scales from years down to a few hours, though the sampling was usually sparse, uneven, or limited in time (Maraschi et al. 1986; Urry et al. 1988; Treves et al. 1989; Edelson et al. 1991; Urry et al. 1993, henceforth U93). The IUE campaign in November 1991 (U93), which was coordinated with ROSAT observations, had adequate time coverage (30 days) and sampling to probe interday variability on an extended time interval, and even intraday variability during the continuous observing period ($\sim$5 days out of 30). The presence of recurrent flares on a $\sim$0.7-day time scale prompted further IUE intensive monitoring in May 1994, coordinated with EUVE (Marshall et al. 1996), ASCA (Kii et al. 1996), and ROSAT (Urry et al. 1996), as well as radio, near-IR, and optical coverage from ground-based telescopes (Pesce et al. 1996). The aim of the IUE campaign was to obtain the longest and best sampled UV light curve ever, in order to test the shortest possible variation time scales, within the capabilities of the IUE instruments, and to explore the correlation with emission at other wavelengths (Urry et al. 1996).

In this paper we concentrate on the IUE monitoring. In § 2 we present the IUE observations and data analysis, in § 3 we describe the UV light curves and spectral variability, in § 4 we discuss these results and in § 5 we summarize our conclusions.

2. Observations and Data Analysis

2.1. Observing Strategy and Spectra Reduction

IUE was scheduled for continuous observations (three 8-hr shifts per day) from 1994 May 15 to 25 inclusive, with 8 brief ($\lesssim 2$ hr) and 5 longer (between 4 and 17 hr) gaps due to Earth occultation and to a few time-critical programs. The target acquisition was done through a double blind offset: first we pointed to the nearby bright star SAO 213406 (V = 6.5, at $44'$ distance from the source), then to the fainter SAO 213450 (V = 9.2, at $4.5'$), and finally to the target itself. The SWP and LWP cameras were exposed in low dispersion mode alternately for 55 and 25 minutes respectively, to achieve comparable signal-to-noise ratio in both cameras, for a typical UV spectral slope of PKS 2155–304 ($\alpha_\nu \simeq 1$). In the absence of operational problems, we obtained one pair of spectra each 96 minutes, due to satellite maneuvering and camera preparation overheads. This time interval was chosen to phase with the ASCA satellite orbital period to allow cleaner cross-correlation analysis between the UV and X-ray light curves; depending on the overheads, some of the spectra had slightly longer or shorter integration times than the nominal 25 and 55 minutes. One long-wavelength spectrum (LWP 28222) and three short-wavelength spectra (SWP 50815, 50840, 50854) were very underexposed (the exposure times were less than half the normal values) and were discarded from the subsequent analysis.

The photometrically flat-fielded and geometrically corrected images were inspected to assure proper target centering. One long-wavelength spectrum was unusable because of

off-axis placement of the aperture during exposure (LWP 28187).

As of late 1992, scattered solar light severely affects the IUE field of view (depending on the satellite position with respect to the Sun) and can significantly compromise the spectrophotometry longwards of ∼2700 Å (Caplinger 1995, and references therein). The scattered light also precludes useful information about the source brightness at optical wavelengths from the FES, so no FES counts from the source were recorded.

Spectra were extracted from each of the 236 good IUE images using the TOMSIPS routine (Ayres 1993; Ayres et al. 1995), a modified version of the Signal-Weighted Extraction Technique (SWET; Kinney, Bohlin, & Neill 1991a). The extracted net fluxes were converted to absolute fluxes using calibration curves based on SWP and LWP low dispersion spectra of the white dwarf WD G191-B2B. No correction was applied for the sensitivity degradation of the cameras. The complete log of the IUE observations is reported in Table 1. Two typical spectra from the campaign are shown in Fig. 1 along with the intrinsic error distribution of the spectral flux. The best-fit power-law model for the continuum is shown as a solid line.

The results of the TOMSIPS extraction were compared with alternative processings using the standard IUESIPS, GEX (Urry & Reichert 1988), and the Final Archive NEWSIPS (Nichols & Linsky 1996). In the first two cases a general consistency was found within ∼10-15%, though GEX gave anomalous results in a few cases. The NEWSIPS LWP spectra from the end of the US2 shift, which is the most heavily affected by background radiation, turned out to be unreliable. For these cases, the signal-to-noise ratio of the spectral data is so low (because of the high background level) that the extraction technique uses only two spline nodes to fit the cross-dispersion profile (Imhoff 1996). In presence of solar light contamination, which ramps up dramatically above 2800 Å, if only two spline nodes are used to fit the cross dispersion profile, the fit cannot accurately follow the rapid

decline in flux below 2800 Å, resulting in overestimated flux in a large portion of the spectrum. For the SWP, the NEWSIPS and TOMSIPS light curves at 1400 Å are in agreement, apart from the different applied calibrations.

The expected interstellar extinction of the UV flux due to Galactic neutral hydrogen is $A_V = 0.08$ mag, corresponding to a column density $N_{HI} = 1.36 \times 10^{20}$ cm^{-2} (Lockman & Savage 1995), assuming a gas-to-dust ratio $N_{HI}/E_{B-V} = 5.2{\times}10^{21}$ cm^{-2} mag^{-1} (Shull & Van Steenberg 1985) and a total-to-selective extinction ratio $A_V/E_{B-V} = 3.1$ (Rieke & Lebofsky 1985). The 236 IUE spectra are well fitted by simple power-law models plus this assumed reddening (§ 2.2). However, with A_V as a free parameter, the χ^2 associated with a power-law model is minimized (both over the full set of SWP and over the set of merged SWP+LWP spectral flux distributions) for $A_V = 0.4$ mag, with a high degree of significance ($> 99.99\%$, according to the F-test). This value is inconsistent with that deduced from the Galactic column density, and in fact with the results from U93, who found no such excess reddening. This might indicate variable absorption at the source or in intervening material (Bruhweiler et al. 1993). Nevertheless, since PKS 2155–304 was observed by EUVE during the campaign (which would have been unlikely if the extinction were so high) and since the $A_V = 0.08$ mag fits are still acceptable, we conservatively adopted $A_V = 0.1$ mag for consistency with U93. (This was derived, under the same above assumptions, from the hydrogen column density determined by the HI 21 cm survey of Stark et al. (1992), $N_{HI} = 1.78 \times 10^{20}$ cm^{-2}.) Note that for $A_V = 0.1$ mag, the SWP+LWP spectral indices are consistent with a simple power-law, while $A_V = 0.4$ mag would require that the SWP slope is steeper by $\Delta\alpha \sim 1$ than the LWP (Fig. 2). For the dereddening corrections we used the extinction curve of Seaton (1979), as in U93. The updated dereddening curve of Cardelli, Clayton, & Mathis (1989) would imply an average discrepancy of the fitted parameters not exceeding their uncertainties.

2.2. Spectral Fitting

For the spectral analysis we followed a procedure similar to U93. Through an iterative, chi-squared minimization fitting routine, the dereddened SWP spectral flux distributions (1230-1950 Å) were fitted in wavelength space to a simple power-law model of the form $F_\lambda \propto \lambda^{-\beta}$, ignoring the regions 1277-1281 Å, 1286-1290 Å, 1660-1666 Å, and 1780-1800 Å, which are affected by camera artifacts (Crenshaw, Bruegman, & Norman 1990), as well as regions of individual spectra contaminated by cosmic ray hits. The fit was normalized to 1560 Å, which is the flux-weighted mean wavelength of the chosen interval for a spectral index $\beta = 1$.

Similarly, power-law spectral fits were made to the LWP spectra in the 2100-2700 Å region, which is not heavily affected by the solar scattered light. Because the signal in the 2700-2800 Å region did not exceed the fit curve extrapolation, and was well represented by the same power-law, we concluded that the effect of the IUE baffle anomaly is negligible shortward of 2800 Å (as suggested also by direct image inspection), so we extended the fitted region to 2800 Å. The fiducial wavelength of the fit normalization, computed as above, was chosen to be 2580 Å.

The 1-σ uncertainties associated with the fitted fluxes are generally less than 1% for SWP spectra, and a few percent for LWP due to the large intrinsic errors affecting the spectral signal between 2100 Å and 2400 Å. To these uncertainties a $\sim$1% photometric error was added in quadrature, following U93 and Edelson et al. (1992). The best-fit parameters, energy spectral indices α (where $\alpha = 2 - \beta$) and fitted fluxes at 1400 Å and 2800 Å (SWP and LWP respectively), are given in Table 1, as are the reduced χ^2 values for each fit (χ^2_ν). We also fitted a power-law model to pairs of SWP and LWP spectra taken close together in time. The fit was done over the wavelength range 1230-2800 Å, excluding the same regions that were discarded in the SWP spectra and the 1900-2150 Å

interval, which is affected by large errors. During the first day of monitoring, the extremely fast variability does not allow any meaningful match between SWP and LWP exposures. Therefore, since the determination of the spectral index would yield unreliable values, due to lack of simultaneity, we excluded the first six pairs of spectra from computation of the combined energy index α_C. The combined SWP+LWP fit results are presented in Table 2.

The present analysis leads to a steeper average spectral slope than reported for the 1991 data ($\langle\alpha_{SWP}\rangle$ is larger by ∼28%, $\langle\alpha_{LWP}\rangle$ by ∼14%, and $\langle\alpha_C\rangle$ by ∼44%), which were reduced with the SWET method. We investigated the cause of this difference by re-analyzing the 1991 data after extracting the spectra with the TOMSIPS routine and found that the change is mostly due to the different adopted calibration curves, and to the fact that the 1991 data were corrected for the SWP camera sensitivity degradation, with smaller effects due to the more limited fitting range at the long wavelengths and (only marginally) to the different extraction algorithms (e.g., profile normalizations). Fitting the 1991 TOMSIPS extracted spectra to a power-law yields average spectral indices that are consistent with those obtained for the 1994 data. (See Table 3 for a synoptic comparison between the 1991 and 1994 sets.)

The average χ^2_ν values for the SWP, LWP, and merged spectral fits are 1.02, 0.67, and 1.00, respectively. This indicates that, given the derived flux errors, the power-law model is acceptable, therefore no rescaling was applied to the intrinsic flux errors (as had been done in U93). To determine errors on spectral index we looked at the differences between spectral indices for pairs of adjacent spectra taken closer in time than 0.1 days, excluding the first six points in each energy index curve (where the variability was much faster than the exposure time), leaving 94, 95, and 91 pairs of SWP, LWP, and merged spectra, respectively.

Assuming that the spectral index does not vary significantly between two observations

spaced only ∼2 hours apart in time (which is not the case in the first part of the monitoring), the difference divided by the sum in quadrature of their individual errors should be normally distributed, with a unity variance. Since we found variances larger than unity (2.13, 1.17, and 2.86 respectively for the SWP, LWP, and merged spectra), we applied, as in U93, a correction to the spectral index errors equivalent to such variance. The spectral index distributions for the SWP and LWP overlap (though the former is much narrower), indicating that the assumed extinction produces a consistent result for both SWP and LWP spectral shapes (see Fig. 2a). For $A_V = 0.4$ mag, the fitted fluxes at 1400 Å and 2800 Å would be larger by ∼110% and ∼65%, respectively, and the mean SWP and LWP spectral indices would be smaller, the differences being ∼0.3 and ∼1.2, respectively, compared to the values given in Table 1 for $A_V = 0.1$ mag. The SWP and LWP spectral index distributions for $A_V = 0.4$ mag (Fig. 2b) differ by $\Delta\alpha \sim 1$, suggesting that such a high extinction value is unlikely.

3. Results

3.1. UV Light Curves

Both long- and short-wavelength IUE light curves clearly show strong fast variability (Fig. 3). The most striking result of the campaign is the high amplitude, extremely rapid flux variability detected during the first day of monitoring (Fig. 3b). At 2800 Å, flux variations as large as a factor 2.2 were found in 1.5 hours (i.e., between one LWP integration and the other), implying that significant variability can occur on time scales shorter than the typical IUE integration time.

The flux at 1400 Å also varied remarkably in the first part of the monitoring, though with smaller observed amplitude (∼25% in 1.5 hours). This behavior is entirely new and

unexpected, since the many previous IUE observations showed only minor differences in SWP and LWP variability, usually in the sense of a larger amplitude in SWP. In Fig. 3b the two light curves are compared normalizing the 2800 Å and the 1400 Å fluxes to their respective mean values (computed excluding the initial flares, i.e. the first six flux points of each curve). The figure shows that the SWP light curve can be reconciled with the hypothesis of a complete correlation with the LWP (i.e., no spectral variability) given that the SWP integrations are twice as long as for the LWP and allowing for the fact that the shortest time scale variability is probably not resolved in either band.

Because the observed variability at 2800 Å is of unprecedented amplitude for such short time scales, we investigated possible extrinsic causes. First, we asked whether motion of the spacecraft could have caused a dip in flux as the source drifted out and back into the large aperture. We examined carefully the line-by-line file for the image with the sharpest drop in spectral flux, LWP 28142. The spectrum is visible with a good signal-to-noise ratio in the central part of the line-by-line image. This, together with proper centering of the adjacent SWP spectra with respect to the geocoronal Ly$_\alpha$ line (which fills the aperture), exclude a drift of the target along the long dimension of the aperture. Similarly, a drift along the dispersion direction is excluded because of the location of the reseau marks at the same wavelengths as in the other images, and the accuracy of the spacecraft slews between the target and the offset star. Second, we ruled out a mis-registration of the Optimal extraction slit with respect to the spectrum, since several independent extraction methods (including the original boxcar) give essentially the same spectrum. Third, this "dip" event might resemble some sudden flux drops detected in LWP data during IUE intensive monitorings, which have been ascribed to voltage failures in the LWP camera (LWP anomaly, T. Teays, private communication, 1996). However, such spurious effects are very rare, and no firm conclusion has been achieved on the correlation between the occurrence of the phenomenon and electric current depletion during the exposure. More importantly, these events are

confined to the LWP, while the event in PKS 2155–304 has a (less dramatic) counterpart in the SWP light curve, in the EUVE light curve (Marshall et al. 1996), and in polarized optical light (Pesce et al. 1996). Considering all these points, we conclude the rapid initial variations reflect actual events in the BL Lac object.

In both light curves, after the very active period recorded at the beginning of the campaign, the flux stays relatively constant (after May 16), with a gentle increase and decline of ∼10% over 3.5 days, and then there is a prominent 2-day flare, with a total increase of ∼35%, starting on May 19. Further variation in the last four days of the monitoring is $\lesssim 20\%$ in both bands. Throughout the monitoring, small (5-10%) and rapid (∼ hours) flux variations are superimposed on the more dramatic flares.

A variability test (Edelson 1992) yields similar variability indices for the SWP and LWP light curves, which are marginally consistent within the 10% error, calculated as in Edelson et al. (1995; $v_i \equiv \frac{\sigma_F}{\langle F \rangle}$, where σ_F is the standard deviation of the flux, and $\langle F \rangle$ its average value): $v_i^{SWP} = 0.11$, $v_i^{LWP} = 0.13$. Performing the test on the light curves after removing their first, dramatically variable portions, results in a 0.10 variability index both for SWP and LWP. This is consistent with the results of the intensive November 1991 campaign on PKS 2155–304, when comparable amplitude variability was found in both IUE wavelength ranges. Systematically larger amplitude variability is found at shorter UV wavelengths than at longer ones for blazars observed over longer time scales (Kinney et al. 1991b; Edelson 1992), but the difference is not significant given the errors (Treves & Girardi 1991), and such differences are not observed on short time scales, where rapid variations are resolved (see U93).

We computed auto- and cross-correlation functions for the light curves by means of the Discrete Correlation Function method (DCF; Edelson & Krolik 1988). Since the character of the variability in the first day is extreme and unresolved, we systematically removed the

first 6 flux points in both light curves prior to application of the DCF routine.

The auto-correlation function of the present SWP and LWP light curves (Fig. 4) does not show any evidence of periodicity (as would be implied by characteristic "humps" on the auto-correlation function curve at non-zero lags) nor is any visible in the light curves, in contrast to the previous findings. The auto-correlation function of a data train shows features at the timescale corresponding to recurrence in its variations, such as periodicity or quasi-periodicity would imply. This allowed U93 to find a quasi-periodic variation in the November 1991 IUE light curves of PKS 2155–304 with a ∼0.7 days time scale (a strict periodicity was shown not to be statistically significant by Edelson et al. 1995). The SWP and LWP light curves are well correlated with each other, with no apparent lag larger than ∼0.1 days (Fig. 5), which is the approximate temporal resolution.

3.2. Spectral Shape and Variability

During the first day of monitoring the UV spectrum of PKS 2155–304 varied both in the LWP and, less prominently, in the SWP range (Fig. 6). After May 16, the slopes of the SWP and LWP spectra have an overall fractional variability $\frac{\sigma_\alpha}{<\alpha>}$ of 0.08 and 0.28, respectively (with a 10% uncertainty on these values), according to the variability test of Edelson (1992). Testing the spectral index behavior against a constant trend yields a χ^2_ν of 1.8 for SWP and 2.2 for LWP, which implies a probability of constancy of less than 0.1%. The central resolved flare is accompanied by spectral variations of more modest amplitude: $\chi^2_\nu \sim 2$ is found for both index curves, whereas $\chi^2_\nu = 53$ and $\chi^2_\nu = 21$ is associated with the flux variations in the SWP and LWP, respectively.

The auto-correlation function of the LWP spectral index shows equally spaced peaks with ∼1 day separation. This periodicity (also recognizable in Fig. 6b) is spurious, deriving

from the periodic background contamination during the US2 shift. The SWP spectral index auto-correlation function does not exhibit any significant features. No clear trend is visible between the fluxes at 1400 Å and the SWP spectral slopes, but their cross-correlation has a minimum at a lag of ~ -1 day (Fig. 7), which implies that spectral flattening (steepening) leads flux increases (decreases). Limiting the cross-correlation function computation to the segments of the light and index curves corresponding to the central flare yields no evidence that the effect might be dominated by the behavior during the outburst.

The slope α_C of the SWP+LWP spectra is significantly variable ($v_i = 0.08$, with $\chi^2_\nu = 2.8$; see Fig. 6c, where α_C is plotted only for observations taken after May 16). During the central flare, a $\chi^2_\nu \simeq 3$ is associated with the α_C variation. Cross-correlating α_C with the flux at 2000 Å yields the same results as found for the SWP: spectral hardening $\sim$1 day in advance of flux rise.

4. Discussion

IUE monitoring of PKS 2155–304 in May 1994 has given us the best sampled UV light curve ever obtained for an AGN, with 2.2 times the temporal extension of the intensive part of the November 1991 campaign. On average, the state presently detected was $\sim$20% lower than in 1991 in both the SWP and the LWP. The observed flux variability behavior was also remarkably different. The light curves from the two intensive campaigns are shown for comparison in Fig. 8. In particular, we do not see the quasi-periodicity seen in 1991 (see flux auto-correlation functions, Fig. 4), which has therefore to be regarded as random or transitory. No significant spectral change is seen between the two epochs (see § 2.2 and Table 3). Compared to the IUE archival data (Edelson et al. 1992; Pian & Treves 1993) both UV flux and spectral index were about average in May 1994.

The 1994 data exhibit dramatic and unprecedented variability, which is still underresolved, during the first day of the monitoring and later a well sampled flare of a factor of ∼35% in ∼1.5 days, visible in both the 1400 Å and 2800 Å light curves without any significant difference. The flux rise to maximum is longer than the fading (∼1 day) toward the previous "quiescent" state (as indicated by the asymmetric shape of the flare, Fig. 3a), in agreement with the finding that UV flux decrease in blazars is usually sharper than brightening (Edelson 1992). The longer and "structured" rise requires that the mechanism producing the flare is not "instantaneous" but rather intrinsically long or diluted, possibly by light travel time effects in the emission region, or by multiple smaller events.

The fast fluctuations seen at the beginning of the light curve are truly exceptional. During the first day the LWP light curve exhibits a variation of a factor 2.2 in 8 hours and a second flare of similar amplitude in 1.5 hours (Fig. 3b). Rapid variability is simultaneously seen in the SWP and in the LWP. Fast (though unresolved) variations have also been detected during the optical observations simultaneous to the present IUE campaign (Pesce et al. 1996). Defining the flux doubling time scale as $\tau = \frac{F_{min}}{F_{max}-F_{min}}\Delta t$ one obtains $\tau_{SWP} =$ 6.87 hr and $\tau_{LWP} = 1.36$ hr as minimum values at 1400 Å and 2800 Å respectively during the monitoring. This is the most rapid observed flux doubling for PKS 2155–304 either in the UV or optical range, where typical values are of the order of days (see U93; Carini & Miller 1992; Miller 1996). Doubling time scales as short as ∼1 hour have been seen in PKS 2155–304 optical light curves (Pesce et al. 1996; Paltani et al. 1996), but for typical amplitudes much smaller than a factor of 2. In X-rays, 1-hour doubling time scales for this source are relatively more common (Morini et al. 1986). Similar events were observed in several X-ray bright blazars in the X-ray band (see e.g., H 0323+022, Feigelson et al. 1986; PKS 2155–304, Treves et al. 1989, Sembay et al. 1993; PKS 0716+714, Cappi et al. 1994), and also in the γ-rays (Mkn 421, Macomb et al. 1995; PKS 1622-297, Mattox et al. 1997).

Conspicuous spectral variations corresponding to the big central flare are not seen, a behavior reminiscent of other BL Lacs in optical and UV (OJ 287, Pian et al. 1996; Sillanpää et al. 1996; PKS 0716+714, Wagner & Witzel 1994, see however Ghisellini et al. 1996, who find opposite results for this object in the optical). This result is to be compared with the outcome of longer term monitorings of blazars (days to years), showing that UV spectral variations do occur but are generally modest compared to flux changes and often weakly or not clearly correlated with them (Edelson 1992; Shrader et al. 1994; Koratkar et al. 1996). Where correlation is found, it is generally in the sense of a harder spectrum for brighter flux (Urry et al. 1988; Bonnell et al. 1994), in qualitative agreement with models based on radiative cooling.

A significant feature of the cross-correlation of flux and spectral index for the SWP (Fig. 7) is a minimum at $\sim$ –1 day, which represents anti-correlation of the two quantities, consistent with the longer term spectral variability mentioned above. The negative time-lag means that the spectrum is hardening (softening) $\sim$1 day before the flux increases (decreases), a result which, as yet unexplained, was also found in the November 1991 campaign (see discussion in U93).

The variability in the initial part of the light curve is so rapid that we cannot test color variations using the joint LWP and SWP ranges during the event. However the spectral index in the LWP range takes one of its lowest values ($\alpha_\nu = 0.5$) and its maximum value ($\alpha_\nu = 1.7$) in correspondence to the relative maximum flux observed on May 15.95 and to the deep minimum observed on May 16.08, respectively. Thus the little information we have points to some spectral variability rather than to an achromatic event.

The completely resolved central flare, together with the $\sim$50% and $\sim$80% correlated flares detected at the extreme UV and X-ray wavelengths, respectively (Marshall et al. 1996; Kii et al. 1996; Urry et al. 1996), is consistent with a variability amplitude monotonically

increasing with energy, as expected for a synchrotron flare in an inhomogeneous jet (Celotti, Maraschi, & Treves 1991; Georganopoulos & Marscher 1996).

The excellent correlation of the SWP and LWP light curves implies that the UV emission in the 1200-3000 Å range is produced within a unique emitting region, without difference in the electron cooling times at these wavelengths larger than an hour. Since these must be equal to or shorter than the UV fading time scales, we can estimate a lower limit for the magnetic field in the UV emitting portion of the jet (Blandford 1990), locally approximated as a homogeneous region:

$$B \geq 1.4 \times \nu_{15}^{-1/3} t_{hr}^{-2/3} (\delta/10)^{-1/3} \qquad G,$$

where ν_{15} is the frequency in units of 10^{15} Hz, t_{hr} is the observed variability timescale in hours, and δ represents the Doppler factor of the relativistic bulk motion. Based on the shortest observed variability time scale (1.5 hr at 2800 Å) and assuming $\delta \sim 10$, we derive $B \geq 1$ G.

The detection of GeV γ-rays from PKS 2155–304 (Vestrand, Stacy, & Sreekumar 1996) indicates that inverse Compton radiation due to electrons scattering off the synchrotron photons or other soft seed photons is significant. The seed photons are expected to emit at optical and UV wavelengths ($\nu_{IC} \sim \gamma^2 \nu_S$, where the maximum electron energy γ is typically $100 - 1000$). Given the derived lower limit on the magnetic field and the measured synchrotron luminosity in the UV (L_S), we can estimate the expected γ-ray luminosity (L_{IC}) in the homogeneous case of an emitting blob of radius $R_{blob} = c t_{var} \delta$. We consider the following relation between the observed synchrotron and inverse Compton luminosities:

$$\frac{L_{IC}}{L_S} \simeq \frac{U_S}{U_B} = \frac{L_S \delta^{-4}}{4\pi R_{blob}^2 c} \cdot \frac{8\pi}{B^2},$$

hence

$$L_{IC} = \frac{2L_S^2}{c^3 B^2 t_{var}^2 \delta^6},$$

where U_B is the magnetic energy density, and U_S is the synchrotron radiation energy density. For $L_S = 1.2 \times 10^{46}$ erg s^{-1}, corresponding to the UV emission alone, and $B \geq 1$ G, $t_{var} = 1.5$ hr, $\delta \sim 10$, one obtains $L_{IC} \leq 3.4 \times 10^{47}$ erg s^{-1}, consistent with the observed γ-ray luminosity of 2.5×10^{45} erg s^{-1}. The only quantities not directly observed are B and δ. The approximation $\delta \sim 10$ is supported by other observations; given the γ-ray limit here, B could be an order of magnitude larger than 1 G.

The extremely rapid variation observed at the beginning of the UV monitoring implies that the limit $\Delta L/\Delta t = 2 \times 10^{42} \eta$ erg s^{-2} (Fabian 1979) is slightly exceeded (by a factor of $\sim$1.2) if an accretion efficiency $\eta = 0.1$ is assumed, for a redshift $z = 0.116$ (Falomo et al. 1993), a Hubble constant $H_0 = 50$ km s^{-1} Mpc^{-1} and a deceleration parameter $q_0 = 0.5$, and hence the rapid variations support the idea of relativistic beaming. Based only on the flux change detected in the 2100-2800 Å band, the beaming factor need not exceed unity, but it might be well larger considering the simultaneous (and in some cases larger) flux variation in other parts of the electromagnetic spectrum, which is unfortunately undersampled (see Urry et al. 1996). The observed time scale corresponds to a very small emission region, only $\sim 10^{14}$ cm if beaming corrections are not applied, or $\sim 10^{15}$ cm for $\delta \simeq 10$. Notice that the constraint on the presence of beaming derived only from the variability in the UV band is a factor of 4 more stringent than found in U93, but weaker than that determined by Morini et al. (1986), who detected a rapid increase in X-ray (1-6 keV) flux for which $\Delta L/\Delta t$ exceeded the above limit by a factor 10.

5. Conclusion

The May 1994 IUE monitoring on PKS 2155–304, which was part of a simultaneous multiwavelength campaign from radio to X-rays, yielded the best sampled UV light curve for this or any blazar and revealed significant flux variability at different time scales, from hours to days. Spectral changes are generally modest and not clearly correlated with flux variations. A resolved central flare of ∼35% amplitude was observed in both IUE cameras, and was likely correlated with flares of different amplitude and duration at higher energies (Urry et al. 1996). The 1.5-hour flux variation of a factor 2.2 seen at 2800 Å during the first day of monitoring is unprecedented for blazars as a class. This event, which suggests the occurrence of variability on time scales even shorter than the IUE time resolution, represents a definite violation of the limits on luminosity variability, therefore implying the presence of relativistic beaming. Both variability events are interpreted within a scenario in which synchrotron radiation is the primary emission mechanism, and a lower limit of 1 G on the intensity of the magnetic field is determined, which turns out to be consistent with a calculation of this physical quantity based on the multiwavelength data and with the γ-ray flux observed by EGRET.

Comparison with the results from the 1991 IUE intensive monitoring of PKS 2155–304 shows that the variability characteristics detected at the two epochs are fundamentally different. In particular, unlike the findings of the 1991 campaign, no periodicity is seen in the present data. The ∼1 day anti-correlation between flux and spectral variations is however maintained.

The fastest variability in the UV has been largely undersampled with IUE for PKS 2155–304, and in general for other blazars. UV telescopes allowing a better time resolution and continuous coverage are clearly needed. Apart from HST, which has rarely been dedicated to long monitorings, none are presently available. While the fast

sporadic variability may be most apparent in the UV, it should be expected to manifest itself, possibly in a less extreme form, also at optical wavelengths. Some indication is already present in the optical data of the 1994 campaign, especially in the polarization measurements (Pesce et al. 1996). These arguments point to the importance of intensive, systematic monitoring in the optical band, possibly with polarization information. Such programs, which have led to the discovery of intraday variability in a number of blazars (Wagner & Witzel 1995; Miller 1996; Sillanpää et al. 1996; Smith 1996), can be carried out with medium sized telescopes and standard instrumentation, but need long, uninterrupted observing runs, possibly coordinated among different sites.

EP, CMU, JEP, and PG acknowledge support from NASA grants NAG5-1034 and NAG5-2499; EP acknowledges support from a NATO-CNR Advanced Fellowship; RIK acknowledges support from NASA LTSA grant NAGW-2120. We are grateful to T. Ayres for clarification of the TOMSIPS routine and to P. Smith for critical comments. The IUE staff at Vilspa and GSFC is acknowledged, and particularly we would like to thank R. Arquilla, R. Bradley, J. Caplinger, D. De Martino, M. England, C. Gonzalez, A. Groebner, C. Imhoff, N. Loiseau, C. Loomis, D. Luthermoser, B. McCollum, J. Nichols, R. Pitts, C. Proffitt, L. Rawley, P. Rodriguez, M. Schlegel, L. Taylor, T. Teays, and R. Thompson for assistance with IUE observations and data reduction. C. Bailyn, R. Bohlin, J. Bregman, W. Brinkmann, M. Carini, L. Chiappetti, M. Donahue, E. Feigelson, A. Fruscione, A. Königl, L. Kedzior, Y. Kondo, A. Koratkar, J. Krolik, A. Lawrence, F. Makino, P. Martin, H. Miller, P. O'Brien, G. Reichert, A. Sadun, M. Sitko, P. Smith, A. Szymkowiak, G. Tagliaferri, E. Tanzi, S. Wagner, R. Warwick, A. Wehrle are acknowledged for their support to the observing project.

Table 1: Log of IUE Observations of PKS 2155–304 and Power-Law Fit Parameters of Dereddened Spectra

IUE Image	Observation Midpoint (UT) (day of May 94)	Exposure Time (min)	Observatory (Goddard or Vilspa)	F_ν^a (mJy)	σ_{F_ν} (mJy)	α_ν^b	σ_{α_ν}	χ^2_ν
SWP 50773	15.71418	60	G	7.03	0.13	0.95	0.10	0.66
SWP 50774	15.78942	55	G	7.75	0.12	0.88	0.07	0.81
SWP 50775	15.85629	35	G	8.66	0.13	1.19	0.06	0.88
SWP 50776	15.98259	45	V	8.95	0.13	1.04	0.05	0.79
SWP 50777	16.05153	44	V	8.63	0.13	1.04	0.06	1.02
SWP 50778	16.11782	55	V	8.01	0.12	0.88	0.05	0.89
SWP 50779	16.18512	55	V	9.89	0.14	0.90	0.05	1.02
SWP 50780	16.25361	55	V	9.92	0.14	0.98	0.05	0.97
SWP 50781	16.32059	50	G	9.90	0.14	0.98	0.05	0.96
SWP 50782	16.38535	55	G	9.89	0.14	0.94	0.05	0.88
SWP 50783	16.45285	55	G	9.91	0.14	1.00	0.05	1.06
SWP 50784	16.51876	55	G	9.86	0.14	1.01	0.05	1.05
SWP 50785	16.58534	55	G	9.91	0.14	0.94	0.05	1.19
SWP 50786	16.65740	42	G	10.19	0.16	0.92	0.08	0.87
SWP 50787	16.71852	55	G	9.72	0.34	0.86	0.25	0.36
SWP 50788	16.78274	45	G	9.85	0.17	1.11	0.09	0.65
SWP 50789	16.84537	40	G	10.34	0.15	0.94	0.05	0.82
SWP 50790	16.98689	48	V	10.11	0.14	1.00	0.05	1.08
SWP 50791	17.05113	55	V	10.15	0.14	0.94	0.05	1.39
SWP 50792	17.11719	55	V	10.17	0.14	0.98	0.05	1.06

Table 1: - *continued.*

IUE Image	Observation Midpoint (UT) (day of May 94)	Exposure Time (min)	Observatory (Goddard or Vilspa)	F_ν^a (mJy)	σ_{F_ν} (mJy)	α_ν^b	σ_{α_ν}	χ^2_ν
SWP 50793	17.18391	55	V	10.05	0.14	1.05	0.05	1.02
SWP 50794	17.25061	55	V	10.21	0.14	0.97	0.05	1.09
SWP 50795	17.31883	55	G	10.37	0.15	0.95	0.05	1.08
SWP 50796	17.38483	55	G	10.24	0.14	1.03	0.05	1.07
SWP 50797	17.45105	53	G	10.33	0.14	1.00	0.05	1.26
SWP 50798	17.51777	55	G	10.25	0.14	1.00	0.05	1.27
SWP 50799	17.58441	55	G	10.42	0.15	0.98	0.05	1.09
SWP 50800	17.65082	55	G	9.96	0.15	1.01	0.07	0.81
SWP 50801	17.71312	40	G	10.02	0.23	0.89	0.15	0.68
SWP 50802	17.77571	30	G	10.03	0.20	1.19	0.12	0.70
SWP 50803	17.84478	35	G	9.89	0.14	1.07	0.06	1.09
SWP 50804	17.97949	40	V	9.59	0.14	1.08	0.06	0.91
SWP 50805	18.04629	55	V	9.93	0.14	1.00	0.05	1.31
SWP 50806	18.10763	40	V	9.61	0.14	1.06	0.06	1.04
SWP 50808	18.38371	55	G	9.56	0.14	1.09	0.05	1.00
SWP 50809	18.44950	57	G	9.50	0.13	1.16	0.05	1.08
SWP 50810	18.51637	55	G	9.44	0.13	1.14	0.05	1.05
SWP 50811	18.58464	53	G	9.46	0.14	1.02	0.05	1.10
SWP 50812	18.65004	55	G	9.40	0.15	0.92	0.07	0.84
SWP 50813	18.70978	35	G	9.08	0.21	1.03	0.15	0.70

Table 1: - *continued.*

IUE Image	Observation Midpoint (UT) (day of May 94)	Exposure Time (min)	Observatory (Goddard or Vilspa)	F_ν^a (mJy)	σ_{F_ν} (mJy)	α_ν^b	σ_{α_ν}	χ^2_ν
SWP 50814	18.77382	33	G	9.59	0.19	0.85	0.12	0.71
SWP 50815[c]	19.00072	17	V	7.75	0.14	1.36	0.10	0.98
SWP 50816	19.05049	55	V	9.28	0.13	1.09	0.05	0.93
SWP 50817	19.11502	50	V	9.23	0.13	1.06	0.05	1.03
SWP 50818	19.18376	55	V	9.39	0.13	1.03	0.05	1.11
SWP 50819	19.24659	47	V	9.51	0.14	1.00	0.06	1.14
SWP 50820	19.32086	42	G	9.22	0.14	1.03	0.06	0.93
SWP 50821	19.38240	58	G	9.49	0.13	0.96	0.05	1.02
SWP 50822	19.44929	57	G	9.38	0.13	1.03	0.05	0.85
SWP 50823	19.51545	56	G	9.68	0.14	0.97	0.05	1.07
SWP 50824	19.58221	58	G	9.76	0.14	0.95	0.05	1.30
SWP 50825	19.64909	54	G	9.59	0.15	0.81	0.07	0.66
SWP 50826	19.70796	33	G	9.20	0.23	0.94	0.17	0.56
SWP 50827	19.77311	40	G	9.37	0.18	1.12	0.11	0.84
SWP 50828	19.84450	40	G	9.51	0.14	0.96	0.05	1.06
SWP 50829	19.98050	43	V	10.04	0.14	1.01	0.05	1.15
SWP 50830	20.04891	48	V	10.45	0.15	0.91	0.05	0.85
SWP 50831	20.11530	53	V	10.72	0.15	0.98	0.05	0.97
SWP 50832	20.18150	51	V	10.95	0.15	0.99	0.05	0.94
SWP 50833	20.24868	53	V	11.12	0.16	0.91	0.05	1.06

Table 1: - *continued.*

IUE Image	Observation Midpoint (UT) (day of May 94)	Exposure Time (min)	Observatory (Goddard or Vilspa)	F_ν^a (mJy)	σ_{F_ν} (mJy)	α_ν^b	σ_{α_ν}	χ^2_ν
SWP 50834	20.31591	55	G	11.05	0.16	0.88	0.05	1.24
SWP 50835	20.38177	57	G	11.16	0.16	0.92	0.05	1.34
SWP 50836	20.44870	58	G	11.03	0.15	1.09	0.05	1.31
SWP 50837	20.51553	57	G	11.23	0.16	0.95	0.05	1.08
SWP 50838	20.58183	56	G	11.37	0.16	1.01	0.05	1.39
SWP 50839	20.64849	54	G	10.69	0.17	1.06	0.08	0.66
SWP 50840[c]	20.70360	23	G	10.99	0.29	1.22	0.18	0.61
SWP 50841	20.77465	35	G	11.62	0.23	0.93	0.12	0.63
SWP 50842	20.84296	40	G	12.47	0.17	1.03	0.05	1.16
SWP 50843	20.98156	50	V	12.44	0.17	1.05	0.04	1.29
SWP 50844	21.04835	55	V	12.68	0.17	1.05	0.04	1.00
SWP 50845	21.11513	55	V	12.66	0.17	1.00	0.04	1.36
SWP 50846	21.18191	55	V	12.87	0.18	0.96	0.04	0.88
SWP 50847	21.24768	52	V	12.90	0.18	0.94	0.05	1.19
SWP 50848	21.31563	55	G	12.82	0.18	0.98	0.04	1.14
SWP 50849	21.38151	53	G	12.48	0.17	1.04	0.05	1.15
SWP 50850	21.44734	55	G	12.39	0.17	0.99	0.05	1.40
SWP 50851	21.51433	56	G	12.60	0.17	0.92	0.04	1.30
SWP 50852	21.58095	54	G	12.49	0.18	0.90	0.05	0.91
SWP 50853	21.64798	52	G	10.98	0.18	1.15	0.08	0.82

Table 1: - *continued.*

IUE Image	Observation Midpoint (UT) (day of May 94)	Exposure Time (min)	Observatory (Goddard or Vilspa)	F_ν^a (mJy)	σ_{F_ν} (mJy)	α_ν^b	σ_{α_ν}	χ^2_ν
SWP 50854[c]	21.70336	23	G	10.81	0.29	1.03	0.18	0.71
SWP 50855	21.77585	35	G	10.51	0.21	1.13	0.12	0.65
SWP 50856	21.84078	30	G	9.99	0.15	1.16	0.06	1.38
SWP 50857	21.98225	50	V	9.72	0.14	1.08	0.05	1.18
SWP 50858	22.04740	53	V	9.61	0.14	1.06	0.05	1.09
SWP 50859	22.11338	45	V	9.01	0.13	1.14	0.06	0.95
SWP 50861	22.38183	55	G	9.05	0.13	1.19	0.05	0.81
SWP 50862	22.44815	55	G	8.95	0.13	1.09	0.05	1.04
SWP 50863	22.51313	55	G	9.13	0.13	1.06	0.05	1.40
SWP 50864	22.57973	55	G	9.33	0.13	0.98	0.05	0.90
SWP 50865	22.64640	55	G	8.83	0.15	0.98	0.09	0.68
SWP 50866	22.70536	35	G	8.87	0.20	1.08	0.15	0.58
SWP 50867	22.77708	48	G	9.00	0.16	0.97	0.09	0.64
SWP 50868	22.83884	30	G	8.61	0.13	1.14	0.07	1.14
SWP 50869	22.98010	52	V	9.71	0.14	1.00	0.05	1.32
SWP 50870	23.04433	45	V	9.78	0.14	1.08	0.05	1.17
SWP 50871	23.11241	55	V	9.85	0.14	1.03	0.05	1.66
SWP 50872	23.18152	53	V	9.83	0.14	1.06	0.05	1.05
SWP 50873	23.24588	50	V	9.73	0.14	1.06	0.05	1.10
SWP 50874	23.31339	55	G	8.90	0.13	1.19	0.05	1.34

Table 1: - *continued.*

IUE Image	Observation Midpoint (UT) (day of May 94)	Exposure Time (min)	Observatory (Goddard or Vilspa)	F_ν^a (mJy)	σ_{F_ν} (mJy)	α_ν^b	σ_{α_ν}	χ^2_ν
SWP 50875	23.37897	55	G	8.88	0.13	1.16	0.05	1.01
SWP 50876	23.44587	55	G	9.31	0.13	1.12	0.05	1.12
SWP 50877	23.51219	55	G	9.71	0.14	1.01	0.05	1.03
SWP 50878	23.57843	55	G	9.85	0.14	1.02	0.05	1.02
SWP 50879	23.64552	55	G	9.04	0.15	1.03	0.08	0.88
SWP 50880	23.70677	40	G	8.53	0.20	1.23	0.15	0.60
SWP 50881	23.77962	52	G	9.06	0.15	0.97	0.08	1.07
SWP 50882	23.83647	30	G	8.58	0.13	1.27	0.06	1.16
SWP 50883	23.97883	55	V	9.99	0.14	1.05	0.05	1.24
SWP 50884	24.04752	55	V	8.96	0.13	1.05	0.05	1.13
SWP 50885	24.11168	55	V	10.07	0.14	1.04	0.05	1.16
SWP 50886	24.17872	55	V	10.30	0.14	1.00	0.05	1.17
SWP 50887	24.24718	50	V	10.18	0.14	1.03	0.05	1.14
SWP 50889	24.71008	55	G	11.31	0.16	1.02	0.05	1.33
SWP 50890	24.77687	55	G	10.87	0.15	1.07	0.04	1.16
SWP 50891	24.83460	30	G	10.51	0.15	1.09	0.06	1.11
SWP 50894	25.71048	55	G	11.13	0.16	0.98	0.05	1.13
SWP 50895	25.77088	37	G	11.09	0.16	1.07	0.06	0.92

Table 1: - *continued.*

IUE Image	Observation Midpoint (UT) (day of May 94)	Exposure Time (min)	Observatory (Goddard or Vilspa)	F_ν^a (mJy)	σ_{F_ν} (mJy)	α_ν^b	σ_{α_ν}	χ^2_ν
LWP 28137	15.67458	30	G	7.75	0.27	0.39	0.35	0.66
LWP 28138	15.75657	30	G	12.04	0.37	0.81	0.29	0.57
LWP 28139	15.83287	25	G	12.07	0.28	0.97	0.21	0.55
LWP 28140	15.95287	25	V	17.68	0.34	0.53	0.15	0.66
LWP 28141	16.02132	25	V	15.12	0.32	1.55	0.18	0.63
LWP 28142	16.08396	25	V	7.87	0.24	1.72	0.30	0.65
LWP 28143	16.15366	25	V	17.54	0.34	1.04	0.15	0.52
LWP 28144	16.22040	25	V	17.30	0.33	0.84	0.15	0.60
LWP 28145	16.28846	25	G	18.23	0.36	1.10	0.16	0.63
LWP 28146	16.35406	25	G	17.72	0.34	0.82	0.15	0.71
LWP 28147	16.42109	25	G	18.02	0.36	1.24	0.16	0.67
LWP 28148	16.48764	25	G	17.43	0.34	1.01	0.16	0.59
LWP 28149	16.55419	25	G	17.96	0.36	0.93	0.16	0.67
LWP 28150	16.62071	25	G	18.54	0.37	0.70	0.16	0.74
LWP 28151	16.68728	25	G	18.94	0.49	0.90	0.23	0.64
LWP 28152	16.75374	25	G	18.37	0.60	0.85	0.32	0.77
LWP 28153	16.81868	20	G	18.94	0.40	1.23	0.18	0.63
LWP 28154	16.95624	25	V	17.91	0.35	1.21	0.15	0.77
LWP 28155	17.01958	25	V	18.89	0.36	1.19	0.15	0.59
LWP 28156	17.08590	25	V	18.33	0.35	1.18	0.15	0.87

Table 1: - *continued.*

IUE Image	Observation Midpoint (UT) (day of May 94)	Exposure Time (min)	Observatory (Goddard or Vilspa)	F_ν^a (mJy)	σ_{F_ν} (mJy)	α_ν^b	σ_{α_ν}	χ^2_ν
LWP 28157	17.15254	25	V	18.09	0.34	1.09	0.15	0.75
LWP 28158	17.21922	25	V	18.37	0.35	1.15	0.15	0.70
LWP 28159	17.28583	25	G	18.61	0.35	0.98	0.15	0.63
LWP 28160	17.35373	25	G	18.27	0.35	0.98	0.15	0.62
LWP 28161	17.42004	25	G	18.67	0.36	1.21	0.15	0.73
LWP 28162	17.48654	25	G	18.58	0.35	0.95	0.15	0.66
LWP 28163	17.55325	25	G	18.67	0.36	0.91	0.15	0.61
LWP 28164	17.61939	25	G	19.01	0.38	0.76	0.16	0.79
LWP 28165	17.68635	25	G	18.74	0.54	0.91	0.27	0.76
LWP 28166	17.75058	20	G	18.85	0.70	0.58	0.36	0.65
LWP 28167	17.81951	25	G	18.99	0.38	0.84	0.16	0.66
LWP 28168	17.95336	25	V	18.43	0.35	1.01	0.15	0.56
LWP 28169	18.01455	25	V	18.50	0.35	1.24	0.15	0.70
LWP 28170	18.08130	25	V	18.17	0.35	1.25	0.15	0.68
LWP 28171	18.35250	25	G	17.31	0.34	0.91	0.16	0.62
LWP 28172	18.41790	25	G	17.72	0.35	1.00	0.16	0.66
LWP 28173	18.48543	25	G	17.28	0.35	1.09	0.16	0.67
LWP 28174	18.55439	25	G	17.40	0.34	0.97	0.16	0.65
LWP 28175	18.61839	25	G	17.89	0.37	1.00	0.17	0.75
LWP 28176	18.68376	20	G	17.81	0.54	0.54	0.29	0.64

Table 1: - *continued.*

IUE Image	Observation Midpoint (UT) (day of May 94)	Exposure Time (min)	Observatory (Goddard or Vilspa)	F_ν^a (mJy)	σ_{F_ν} (mJy)	α_ν^b	σ_{α_ν}	χ^2_ν
LWP 28177	18.74965	20	G	16.62	0.60	–0.13	0.35	0.55
LWP 28183	19.01873	25	V	17.09	0.34	1.24	0.16	0.63
LWP 28184	19.08539	25	V	17.10	0.34	1.22	0.16	0.60
LWP 28185	19.15266	25	V	16.75	0.33	1.10	0.16	0.66
LWP 28186	19.21819	25	V	16.81	0.33	0.83	0.16	0.59
LWP 28188	19.35045	25	G	16.78	0.33	0.79	0.16	0.59
LWP 28189	19.41771	25	G	16.89	0.34	0.90	0.16	0.58
LWP 28190	19.48420	25	G	16.67	0.33	1.03	0.16	0.60
LWP 28191	19.54995	25	G	17.36	0.34	1.08	0.16	0.57
LWP 28192	19.61765	25	G	16.86	0.34	0.41	0.16	0.63
LWP 28193	19.68391	25	G	16.82	0.52	0.34	0.29	0.59
LWP 28194	19.74867	23	G	17.99	0.75	1.17	0.42	0.65
LWP 28195	19.81773	18	G	18.05	0.36	0.79	0.16	0.66
LWP 28196	19.95100	25	G	17.67	0.34	0.88	0.15	0.60
LWP 28197	20.01746	25	V	18.56	0.35	1.02	0.15	0.71
LWP 28198	20.08449	25	V	18.88	0.36	1.00	0.15	0.64
LWP 28199	20.15042	25	V	18.81	0.35	1.04	0.15	0.63
LWP 28200	20.21753	25	V	19.57	0.37	0.91	0.15	0.61
LWP 28201	20.28340	25	V	19.26	0.37	0.71	0.15	0.64
LWP 28202	20.35010	25	G	19.69	0.38	0.82	0.15	0.66

Table 1: - *continued.*

IUE Image	Observation Midpoint (UT) (day of May 94)	Exposure Time (min)	Observatory (Goddard or Vilspa)	F_ν^a (mJy)	σ_{F_ν} (mJy)	α_ν^b	σ_{α_ν}	χ^2_ν
LWP 28203	20.41673	25	G	20.28	0.38	1.07	0.14	0.68
LWP 28204	20.48396	25	G	20.07	0.37	0.83	0.14	0.55
LWP 28205	20.55041	25	G	20.07	0.37	0.89	0.14	0.66
LWP 28206	20.61706	25	G	20.62	0.41	0.68	0.16	0.72
LWP 28207	20.68032	25	G	22.14	0.77	0.94	0.34	0.63
LWP 28208	20.74675	16	G	20.73	0.83	0.12	0.39	0.65
LWP 28209	20.81692	15	G	22.24	0.43	0.43	0.15	0.64
LWP 28210	20.94994	25	G	23.09	0.41	1.01	0.13	0.59
LWP 28211	21.01677	25	V	22.71	0.40	0.83	0.13	0.65
LWP 28212	21.08339	25	V	22.82	0.40	0.89	0.13	0.80
LWP 28213	21.15039	25	V	23.02	0.41	1.03	0.13	0.68
LWP 28214	21.21723	25	V	22.82	0.41	0.88	0.13	0.66
LWP 28215	21.28325	25	V	22.70	0.41	0.81	0.13	0.66
LWP 28216	21.35069	25	G	22.91	0.41	0.96	0.13	0.68
LWP 28217	21.41593	25	G	22.44	0.40	0.77	0.13	0.53
LWP 28218	21.48215	25	G	22.27	0.40	0.87	0.13	0.74
LWP 28219	21.54946	25	G	22.25	0.40	0.71	0.13	0.56
LWP 28220	21.61635	25	G	21.59	0.41	0.25	0.15	0.91
LWP 28221	21.67990	25	G	22.72	0.75	0.91	0.32	0.64
LWP 28222[c]	21.74510	16	G	21.35	0.96	1.16	0.45	0.61

Table 1: - *continued.*

IUE Image	Observation Midpoint (UT) (day of May 94)	Exposure Time (min)	Observatory (Goddard or Vilspa)	F_ν^a (mJy)	σ_{F_ν} (mJy)	α_ν^b	σ_{α_ν}	χ^2_ν
LWP 28223	21.81732	13	G	19.85	0.40	0.45	0.16	0.63
LWP 28224	21.95083	25	G	18.65	0.35	1.12	0.15	0.58
LWP 28225	22.01694	25	V	18.46	0.35	1.14	0.15	0.64
LWP 28226	22.08223	25	V	18.07	0.36	1.30	0.16	0.70
LWP 28227	22.34867	25	V	17.06	0.34	1.09	0.16	0.61
LWP 28228	22.41740	25	G	17.44	0.35	1.24	0.16	0.73
LWP 28229	22.48184	25	G	17.45	0.35	1.52	0.17	0.65
LWP 28230	22.54847	25	G	17.18	0.34	1.17	0.16	0.65
LWP 28231	22.61508	25	G	17.92	0.38	0.73	0.18	0.80
LWP 28232	22.67991	25	G	17.64	0.56	0.80	0.31	0.79
LWP 28233	22.74640	20	G	17.19	0.65	0.96	0.38	0.69
LWP 28234	22.81508	18	G	17.28	0.34	0.73	0.15	0.74
LWP 28235	22.94809	25	G	17.63	0.34	1.04	0.15	0.63
LWP 28236	23.01624	25	V	18.14	0.34	0.87	0.15	0.69
LWP 28237	23.06579	25	V	18.45	0.35	1.30	0.15	0.73
LWP 28238	23.14927	25	V	18.25	0.35	1.14	0.15	0.73
LWP 28239	23.21620	25	V	18.34	0.35	1.09	0.15	0.55
LWP 28240	23.28145	25	V	17.83	0.35	0.92	0.15	0.69
LWP 28241	23.34773	25	G	18.28	0.35	1.20	0.15	0.72
LWP 28242	23.41432	25	G	18.16	0.35	1.24	0.16	0.67

Table 1: - *continued.*

IUE Image	Observation Midpoint (UT) (day of May 94)	Exposure Time (min)	Observatory (Goddard or Vilspa)	F_ν^a (mJy)	σ_{F_ν} (mJy)	α_ν^b	σ_{α_ν}	χ^2_ν
LWP 28243	23.48093	25	G	18.39	0.35	1.26	0.15	0.71
LWP 28244	23.54752	25	G	18.39	0.36	1.28	0.16	0.63
LWP 28245	23.61417	25	G	18.15	0.37	0.74	0.17	0.77
LWP 28246	23.68069	25	G	17.59	0.54	0.52	0.29	0.69
LWP 28247	23.74660	25	G	18.83	0.58	0.85	0.29	0.54
LWP 28248	23.81392	21	G	18.95	0.36	1.12	0.15	0.54
LWP 28249	23.94704	25	G	18.69	0.36	1.18	0.15	0.64
LWP 28250	24.01432	25	V	18.64	0.35	1.17	0.15	0.69
LWP 28251	24.08010	25	V	18.85	0.36	1.28	0.15	0.74
LWP 28252	24.14703	25	V	18.66	0.35	1.06	0.15	0.66
LWP 28253	24.21411	25	V	19.57	0.37	1.35	0.15	0.79
LWP 28254	24.28127	25	V	19.09	0.36	1.14	0.15	0.84
LWP 28256	24.67891	25	V	20.00	0.37	0.81	0.14	0.80
LWP 28257	24.74557	25	G	20.43	0.38	0.80	0.14	0.77
LWP 28258	24.81200	25	G	20.66	0.38	1.30	0.14	0.68
LWP 28259	24.94266	25	G	19.59	0.42	1.16	0.18	0.57
LWP 28262	25.67900	17	G	20.34	0.39	0.52	0.15	0.66
LWP 28263	25.74547	25	G	20.86	0.40	0.65	0.15	0.62

Note.- The number of degrees of freedom for the fits is typically 410 for the SWP and 264 for the LWP.

[a] At 1400 Å or 2800 Å for SWP or LWP spectra, respectively.

[b] Fitted ranges are 1230-1950 Å and 2100-2800 Å for SWP and LWP spectra, respectively.

[c] Underexposed spectrum.

Table 2: Power-Law Fit Parameters of Merged SWP-LWP Spectra

Spectral Pair Image Numbers		Observation Midpoint (UT)	F_{2000} (mJy)	$\sigma_{F_{2000}}$ (mJy)	α_C	σ_{α_C}	χ^2_ν
SWP	LWP	(Day of May 94)					
50779	28143	16.16939	13.32	0.18	0.83	0.04	0.88
50780	28144	16.23701	13.43	0.18	0.84	0.04	0.95
50781	28145	16.30453	13.60	0.18	0.88	0.04	0.90
50782	28146	16.36971	13.51	0.18	0.87	0.04	0.85
50783	28147	16.43697	13.49	0.18	0.85	0.04	1.06
50784	28148	16.50320	13.38	0.18	0.84	0.04	1.03
50785	28149	16.56976	13.54	0.19	0.87	0.04	1.00
50786	28150	16.63905	14.01	0.20	0.89	0.05	0.85
50787	28151	16.70290	13.75	0.22	0.96	0.07	0.49
50788	28152	16.76824	13.92	0.22	0.95	0.07	0.74
50789	28153	16.83202	14.07	0.19	0.86	0.04	0.81
50790	28154	16.97156	13.62	0.18	0.82	0.04	1.16
50791	28155	17.03536	13.95	0.19	0.89	0.04	1.15
50792	28156	17.10154	13.79	0.18	0.84	0.04	1.12
50793	28157	17.16822	13.75	0.18	0.86	0.04	1.12
50794	28158	17.23492	13.84	0.19	0.84	0.04	1.03
50795	28159	17.30233	14.11	0.19	0.86	0.04	0.98
50796	28160	17.36928	14.01	0.19	0.86	0.04	1.07
50797	28161	17.43554	14.05	0.19	0.85	0.04	1.21
50798	28162	17.50215	14.10	0.19	0.88	0.04	1.15
50799	28163	17.56883	14.25	0.19	0.87	0.04	1.00
50800	28164	17.63511	14.03	0.20	0.96	0.04	0.81

Table 2: - *continued*

Spectral Pair Image Numbers		Observation Midpoint (UT)	F_{2000} (mJy)	$\sigma_{F_{2000}}$ (mJy)	α_C	σ_{α_C}	χ^2_ν
SWP	LWP	(Day of May 94)					
50801	28165	17.69974	13.85	0.23	0.90	0.08	0.70
50802	28166	17.76314	14.42	0.25	1.00	0.09	0.70
50803	28167	17.83215	14.11	0.19	0.98	0.04	0.98
50804	28168	17.96642	13.56	0.18	0.96	0.04	0.85
50805	28169	18.03042	13.70	0.18	0.89	0.04	1.20
50806	28170	18.09446	13.34	0.18	0.91	0.04	1.03
50808	28171	18.36811	13.25	0.18	0.90	0.04	1.02
50809	28172	18.43370	13.41	0.18	0.95	0.04	1.14
50810	28173	18.50090	13.13	0.18	0.90	0.04	1.16
50811	28174	18.56951	13.07	0.18	0.90	0.04	1.00
50812	28175	18.63421	13.05	0.18	0.92	0.04	0.83
50813	28176	18.69677	13.14	0.22	1.02	0.08	0.70
50814	28177	18.76174	13.09	0.22	0.88	0.09	0.68
50816	28183	19.03461	12.81	0.17	0.89	0.04	1.03
50817	28184	19.10021	12.74	0.17	0.89	0.04	1.01
50818	28185	19.16821	12.79	0.17	0.85	0.04	1.12
50819	28186	19.23239	12.96	0.18	0.85	0.04	1.03
50821	28188	19.36642	12.92	0.18	0.86	0.04	0.93
50822	28189	19.43350	12.90	0.18	0.88	0.04	0.86
50823	28190	19.49983	12.98	0.18	0.81	0.04	1.05
50824	28191	19.56608	13.20	0.18	0.84	0.04	1.13
50825	28192	19.63337	13.04	0.18	0.86	0.05	0.65

Table 2: - *continued*

Spectral Pair Image Numbers		Observation Midpoint (UT)	F_{2000} (mJy)	$\sigma_{F_{2000}}$ (mJy)	α_C	σ_{α_C}	χ^2_ν
SWP	LWP	(Day of May 94)					
50826	28193	19.69594	12.84	0.22	0.93	0.09	0.58
50827	28194	19.76089	13.21	0.23	0.96	0.09	0.73
50828	28195	19.83112	13.37	0.18	0.95	0.04	0.90
50829	28196	19.96575	13.60	0.18	0.84	0.04	1.01
50830	28197	20.03319	14.08	0.19	0.83	0.04	0.86
50831	28198	20.09990	14.49	0.19	0.83	0.04	0.99
50832	28199	20.16596	14.58	0.20	0.79	0.04	1.01
50833	28200	20.23311	15.03	0.20	0.83	0.04	0.93
50834	28201	20.29966	14.88	0.20	0.83	0.04	1.05
50835	28202	20.36594	15.13	0.20	0.84	0.04	1.14
50836	28203	20.43272	15.33	0.20	0.91	0.04	1.29
50837	28204	20.49974	15.37	0.20	0.87	0.04	0.94
50838	28205	20.56612	15.48	0.21	0.86	0.04	1.26
50839	28206	20.63278	15.26	0.21	0.99	0.05	0.72
50841	28208	20.76070	16.20	0.28	0.92	0.09	0.65
50842	28209	20.82994	17.44	0.23	0.93	0.04	1.02
50843	28210	20.96575	17.31	0.23	0.91	0.03	1.18
50844	28211	21.03256	17.49	0.23	0.89	0.03	1.06
50845	28212	21.09926	17.41	0.23	0.88	0.03	1.28
50846	28213	21.16615	17.44	0.23	0.84	0.03	0.90
50847	28214	21.23246	17.46	0.23	0.84	0.04	1.06
50848	28215	21.29944	17.52	0.23	0.86	0.03	1.06

Table 2: - *continued*

Spectral Pair Image Numbers		Observation Midpoint (UT)	F_{2000} (mJy)	$\sigma_{F_{2000}}$ (mJy)	α_C	σ_{α_C}	χ^2_ν
SWP	LWP	(Day of May 94)					
50849	28216	21.36610	17.28	0.23	0.90	0.03	1.09
50850	28217	21.43163	17.10	0.23	0.90	0.04	1.16
50851	28218	21.49824	17.04	0.22	0.84	0.03	1.16
50852	28219	21.56520	16.99	0.23	0.86	0.04	0.80
50853	28220	21.63216	16.16	0.23	1.07	0.05	0.93
50856	28223	21.82905	14.75	0.20	1.08	0.04	1.17
50857	28224	21.96654	13.73	0.19	0.95	0.04	1.06
50858	28225	22.03217	13.54	0.18	0.95	0.04	1.01
50859	28226	22.09781	12.92	0.18	1.00	0.04	0.96
50861	28227	22.36525	12.75	0.17	0.94	0.04	0.94
50862	28228	22.43277	12.69	0.17	0.96	0.04	1.03
50863	28229	22.49748	12.70	0.17	0.91	0.04	1.27
50864	28230	22.56410	12.81	0.17	0.88	0.04	0.86
50865	28231	22.63074	12.81	0.18	1.05	0.05	0.72
50866	28232	22.69263	12.81	0.22	1.02	0.09	0.67
50867	28233	22.76174	12.60	0.20	0.94	0.08	0.69
50868	28234	22.82696	12.55	0.17	1.05	0.04	1.01
50869	28235	22.96410	13.32	0.18	0.88	0.04	1.19
50870	28236	23.03028	13.68	0.18	0.93	0.04	1.10
50871	28237	23.08910	13.64	0.18	0.90	0.04	1.47
50872	28238	23.16539	13.63	0.18	0.90	0.04	1.07
50873	28239	23.23104	13.61	0.18	0.93	0.04	0.98

Table 2: - *continued*

Spectral Pair Image Numbers		Observation Midpoint (UT)	F_{2000} (mJy)	$\sigma_{F_{2000}}$ (mJy)	α_C	σ_{α_C}	χ^2_ν
SWP	LWP	(Day of May 94)					
50874	28240	23.29742	12.95	0.18	1.04	0.04	1.18
50875	28241	23.36335	12.95	0.17	1.05	0.04	0.98
50876	28242	23.43009	13.23	0.18	0.97	0.04	1.08
50877	28243	23.49656	13.46	0.18	0.91	0.04	0.99
50878	28244	23.56297	13.58	0.18	0.89	0.04	0.99
50879	28245	23.62984	13.08	0.19	1.03	0.05	0.86
50880	28246	23.69373	12.73	0.21	1.11	0.08	0.67
50881	28247	23.76311	13.20	0.20	1.06	0.07	0.90
50882	28248	23.82520	13.05	0.18	1.16	0.04	0.97
50883	28249	23.96293	13.88	0.18	0.91	0.04	1.14
50884	28250	24.03092	13.03	0.17	1.05	0.04	0.97
50885	28251	24.09589	13.91	0.18	0.90	0.04	1.14
50886	28252	24.16287	14.12	0.19	0.87	0.04	1.10
50887	28253	24.23064	14.17	0.19	0.92	0.04	1.12
50889	28256	24.69450	15.47	0.21	0.86	0.04	1.28
50890	28257	24.76122	15.38	0.20	0.96	0.03	1.11
50891	28258	24.82330	14.85	0.20	0.96	0.04	1.04
50894	28262	25.69474	15.53	0.21	0.93	0.04	0.98
50895	28263	25.75818	15.74	0.21	0.97	0.04	0.85

Note.- The number of degrees of freedom for the fits is typically 625.

Table 3: Comparison between SWET and TOMSIPS Extractions

Range	Average Spectral Indices		
	1991, SWET[a]	1991, TOMSIPS	1994, TOMSIPS
1230-1950 Å	0.80±0.06[b] (98[c])	0.91±0.06 (98)	1.02±0.08 (115)
2100-2800 Å	–	0.94±0.13 (97)	0.95±0.28 (117)
2100-3100 Å	0.83±0.12 (97)	0.83±0.10 (97)	–
1230-2800 Å	–	0.83±0.04 (99)	0.91±0.07 (107)
1230-3100 Å	0.63±0.04 (99)	0.81±0.04 (99)	–

[a] Results from U93.

[b] Standard deviation with respect to the mean. Typical errors on individual spectral indices of the November 1991 campaign were 0.05 for SWP, 0.1 for LWP and 0.02 for merged spectra.

[c] Number of spectra.

REFERENCES

Allen, R. G., Smith, P. S., Angel, J. R. P., Miller, B. W., Anderson, S. F., & Margon, B. 1993, ApJ, 403, 610

Ayres, T. R. 1993, PASP, 105, 538

Ayres, T. R., et al. 1995, ApJS, 96, 223

Blandford, R. D. 1990, in Active Galactic Nuclei, Eds. T. J.-L. Courvoisier and M. Mayor (Berlin: Springer Verlag), p. 168

Bonnell, J. T., Vestrand, W. T., & Stacy, J. G. 1994, ApJ, 420, 545

Bregman, J. N. 1990, A&AR, 2, 125

Bruhweiler, F. C., Boggess, A., Norman, D. J., Grady, C. A., Urry, C. M., & Kondo, Y. 1993, ApJ, 409, 199

Caplinger, J. 1995, NASA IUE Newsletter No. 55, 17

Cappi, M., Comastri, A., Molendi, S., Palumbo, G. G. C., Della Ceca, R., & Maccacaro, T. 1994, MNRAS, 271, 438

Cardelli, J. A., Clayton, G. C., & Mathis, J. S. 1989, ApJ, 345, 245

Carini, M., & Miller, H. R. 1992, ApJ, 385, 146

Celotti, A., Maraschi, L., & Treves, A. 1991, ApJ, 377, 403

Crenshaw, M. D., Bruegman, O. W., & Norman, D. J. 1990, PASP, 102, 463

Edelson, R. A., & Krolik, J. H. 1988, ApJ, 333, 646

Edelson, R. A., et al. 1991, ApJ, 372, L9

Edelson, R. A. 1992, ApJ, 401, 516

Edelson, R. A., Pike, G. F., Saken, J. M., Kinney, A., & Shull, J. M. 1992, ApJS, 83, 1

Edelson, R. A., et al. 1995, ApJ, 438, 120

Fabian, A. C. 1979, Proc. Roy. Soc., 366, 449

Falomo, R., Pesce, J. E., & Treves 1993, ApJ, 411, L63

Feigelson, E. D., et al. 1986, ApJ, 302, 337

Georganopoulos, M., & Marscher, A. P. 1996, in Proc. of the Workshop on Blazar Continuum Variability, Miami, February 1996, p. 262

Ghisellini, G., Maraschi, L., & Treves, A. 1985, A&A, 146, 204

Ghisellini, G., et al. 1997, A&A, accepted

Hutter, D. J., & Mufson, S. L. 1986, ApJ, 301, 50

Imhoff, C. 1996, IUE NASA Newsletter, 56, 108

Kii, T., et al. 1996, in preparation

Kinney, A. L., Bohlin, R. C., & Neill, J. D. 1991a, PASP, 103, 694

Kinney, A. L., Bohlin, R. C., Blades, J. C., & York, D. G. 1991b, ApJS, 75, 645

Königl, A. 1981, ApJ, 243, 700

Koratkar, A. P., Pesce, J. E., Urry, C. M., & Pian, E. 1996, ApJ, submitted

Lockman, F. J., & Savage, B. D. 1995, ApJS, 97, 1

Macomb, D. J., et al. 1995, ApJ, 449, L99

Maraschi, L., Tagliaferri, G., Tanzi, E. G., & Treves, A. 1986, ApJ, 304, 637

Marscher, A. P. 1980, ApJ, 235, 386

Marshall, H., et al. 1996, in preparation

Mattox, J. R., Wagner, S. J., Malkan, M., McGlynn, T. A., Schachter, J. F., Grove, J. E., Johnson, W. N., & Kurfess, J. D. 1997, ApJ, 476, 692

Miller, H. R., & Noble, J. C. 1996, in Blazar Continuum Variability, ASP Conf. Ser. Vol. 110, eds H. R. Miller, J. R. Webb, and J. C. Noble, p. 17

Morini, M., et al. 1986, ApJ, 306, L71

Nichols, J. S., & Linsky, J. L. 1996, AJ, 111, 517

Paltani, S., Courvoisier, T. J.-L., Bratschi, P., & Blecha, A. 1996, Proc. of the Workshop on Blazar Continuum Variability, Miami, February 1996, p. 36

Pesce, J. E., et al. 1997, ApJ, in press

Pian, E., & Treves, A. 1993, ApJ, 416, 130

Pian, E., Treves, A., Webb, J., Kazanas, D., Maraschi, L., McCollum, B., Shrader, C., & Wamsteker, W. 1996, Proceedings of the OJ-94 Project Meeting, Tuorla Observatory Reports, No. 176, Ed. L. O. Takalo, p. 26

Rieke, G. H., & Lebofsky, M. J. 1985, ApJ, 288, 618

Seaton, M. J. 1979, MNRAS, 187, 73p

Sembay, S., Warwick, R. S., Urry, C. M., Sokoloski, J., George, I. M., Makino, F., & Ohashi, T. 1993, ApJ, 404, 112

Shrader, C. R., et al. 1994, AJ, 107, 904

Shull, J. M., & Van Steenberg, M. E. 1985, ApJ, 294, 599

Sillanpää, A. 1996, Proc. of the Workshop on Blazar Continuum Variability, Miami, February 1996, p. 74

Smith, P. S. 1996, Proc. of the Workshop on Blazar Continuum Variability, Miami, February 1996, p. 135

Stark, A. A., Gammie, C. F., Wilson, R. W., Bally, J., Linke, R. A., Heiles, C., & Hurwitz, M. 1992, ApJS, 79, 77

Treves, A., et al. 1989, ApJ, 341, 733

Treves, A., & Girardi, E. 1991, in Variability of Active Galaxies, eds. W. J. Duschl, S. J. Wagner, and M. Camenzind, Lecture Notes in Physics, 377 (Springer Verlag: Berlin), p. 175

Urry, C. M., Kondo, Y., Hackney, K. R. H., & Hackney, R. L. 1988, ApJ, 330, 791

Urry, C. M., & Reichert, G. A. 1988, IUE NASA Newsletter, 34, 95

Urry, C. M., et al. 1993, ApJ, 411, 614 (U93)

Urry, C. M., et al. 1997, ApJ, in press

Vestrand, W. T., Stacy, J. G., & Sreekumar, P. 1996, ApJ, 454, L93

Wagner, S. J., & Witzel, A. 1994, in The Nature of Compact Objects in Active Galactic Nuclei, Proc. of the 33rd Herstmonceux Conference, Eds. A. Robinson and R. Terlevich, Cambridge University Press, p. 397

Wagner, S. J., & Witzel, A. 1995, ARAA, 33, 163

Wandel, A., & Urry, C. M. 1991, ApJ, 367, 78

Figure Captions

Fig. 1 – Typical spectra from the May 1994 IUE campaign not corrected for reddening (upper panels). In both cases the power-law fitting curve $F_\lambda \propto \lambda^{-\beta}$ is shown as a solid line, with indices *a)* $\beta = 0.92 \pm 0.03$; *b)* $\beta = 0.76 \pm 0.13$. The lower panels represent the intrinsic error distributions of the spectral fluxes.

Fig. 2 – Histograms of dereddened SWP (solid line) and LWP (dashed line) spectral indices for *a)* $A_V = 0.1$ mag; *b)* $A_V = 0.4$ mag.

Fig. 3 – Dereddened light curves at 1400 Å (filled circles) and 2800 Å (open circles): *a)* full observing period (the circled points correspond to underexposed spectra, see text); *b)* expanded view of the initial portion. In the second plot, the light curves are normalized to their respective averages, calculated after excluding the flux points taken during the first day of monitoring. Variability is detected on time scales comparable to the exposure times (up to a factor $\sim$2.2 flux change at 2800 Å in 1.5 hr), and more rapid variations are probably present but unresolved.

Fig. 4 – Auto-correlation function of the 1400 Å flux (filled circles) and the 2800 Å flux (open circles) computed with the DCF of Edelson & Krolik (1988).

Fig. 5 – Cross-correlation function between the 1400 Å and 2800 Å light curves computed with the DCF of Edelson & Krolik (1988).

Fig. 6 – Spectral indices for the dereddened flux distributions in the *a)* 1230-1950 Å band; *b)* 2100-2800 Å band; *c)* 1230-2800 Å band. The circled points correspond to underexposed spectra. The horizontal solid lines represent the average energy indices in each band.

Fig. 7 – Cross-correlation function between the flux at 1400 Å and the SWP spectral

index computed with the DCF of Edelson & Krolik (1988). The spectrum flattens ∼1 day before the flux increases.

Fig. 8 – Comparison of the light curves at 1400 Å (filled) and at 2800 Å (open) obtained during the present IUE campaign (circles) and during the intensive monitoring period in November 1991 (squares). Day 1 in the temporal scale corresponds to 10 November for the 1991 data and to 15 May for the 1994 data. For both epochs, the light curves have been normalized to the average SWP and LWP fluxes in 1991. The flux level in 1991 was ∼20% brighter than in 1994. The character of the variability is different at the two epochs: recurrent ∼20% variations detected in 1991 are not seen in the 1994 data, which exhibit an extremely rapid flux doubling at the beginning of the light curve and a big central flare of ∼35% amplitude.

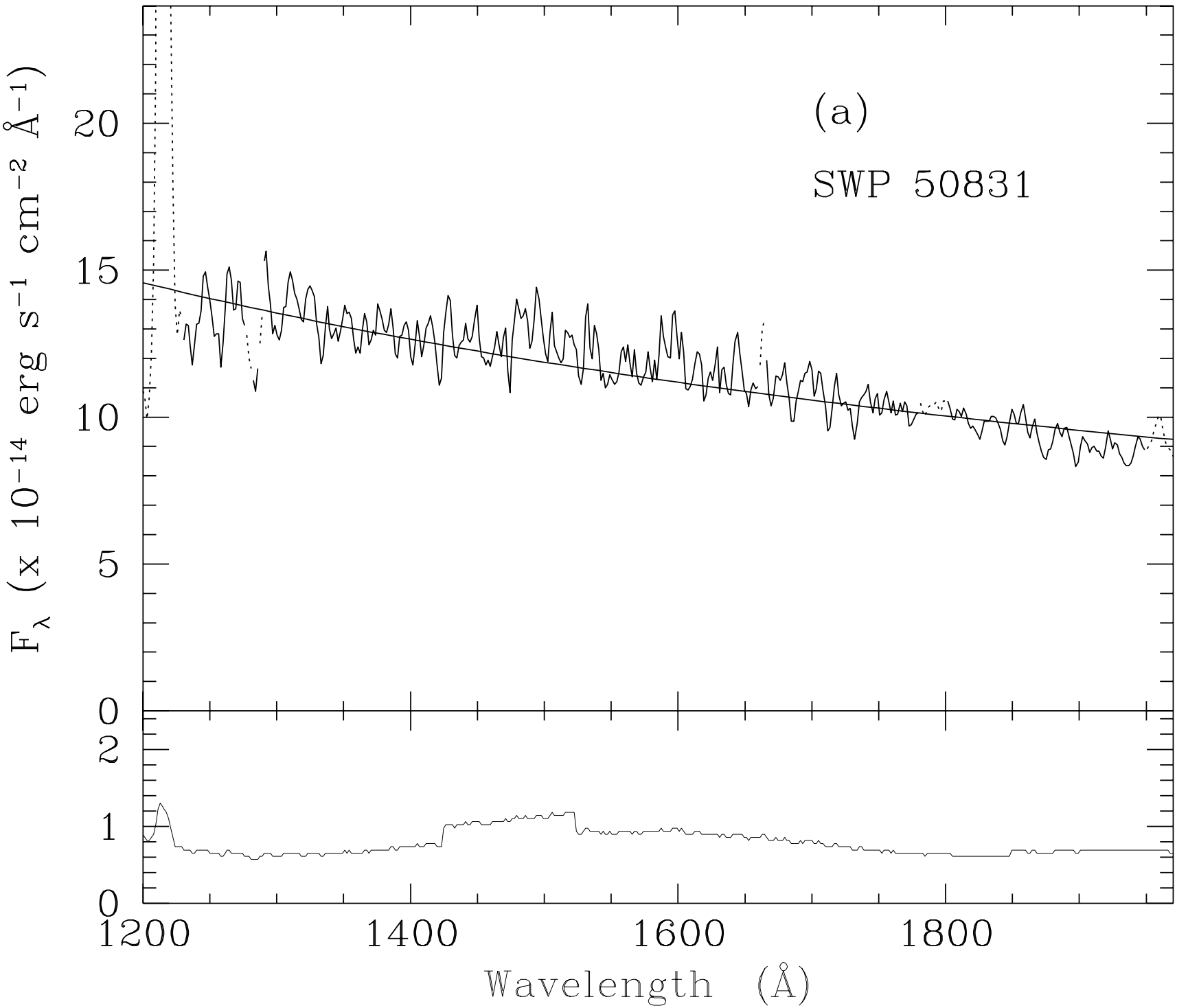
(a)
SWP 50831
F_λ (x 10^{-14} erg s^{-1} cm^{-2} Å^{-1})
20
15
10
5
0
2
1
0
1200
1400
1600
1800
Wavelength (Å)

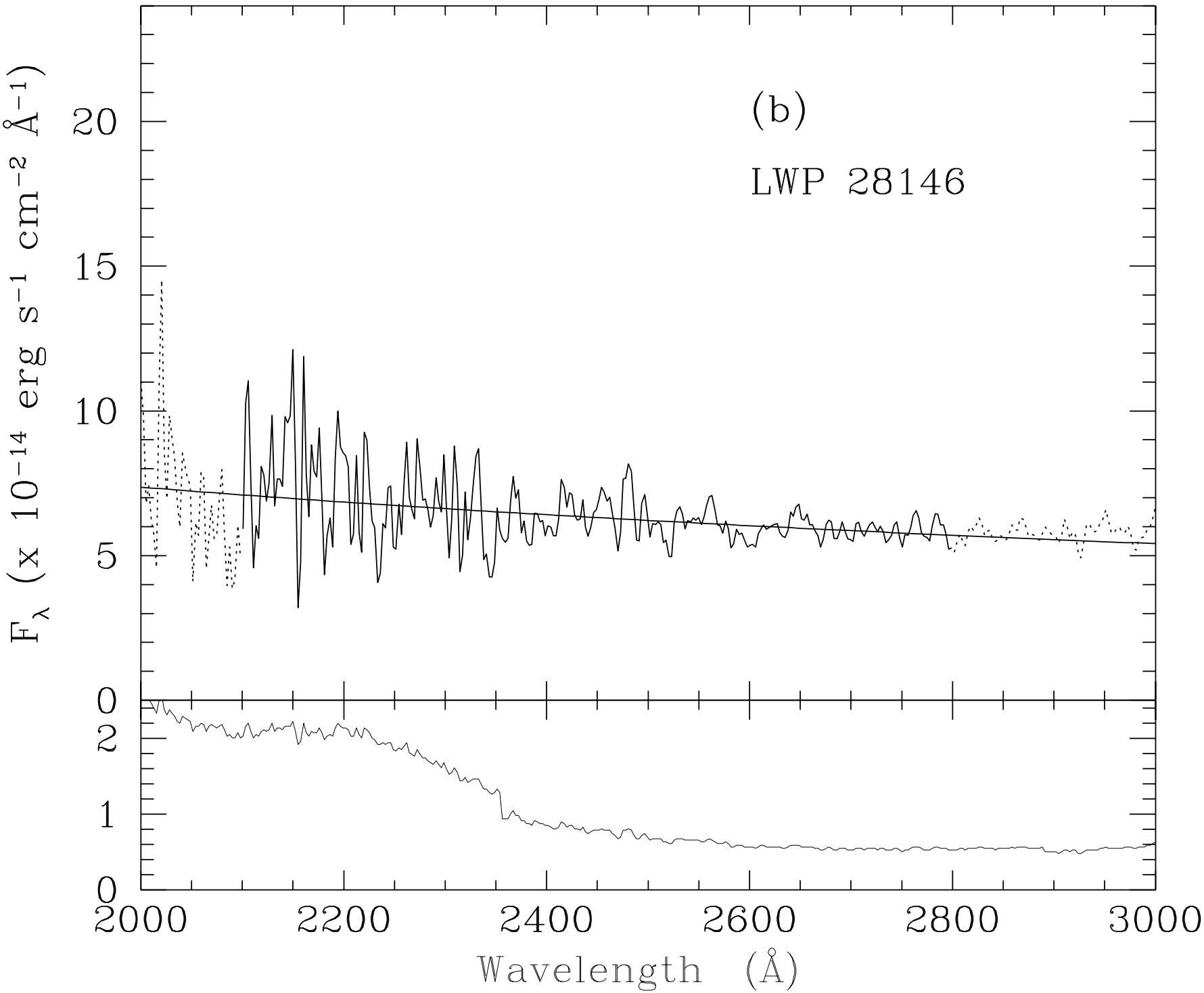
(b)
LWP 28146
F_λ (x 10^{-14} erg s^{-1} cm^{-2} Å^{-1})
0
5
10
15
20
0
1
2
2000
2200
2400
2600
2800
3000
Wavelength (Å)

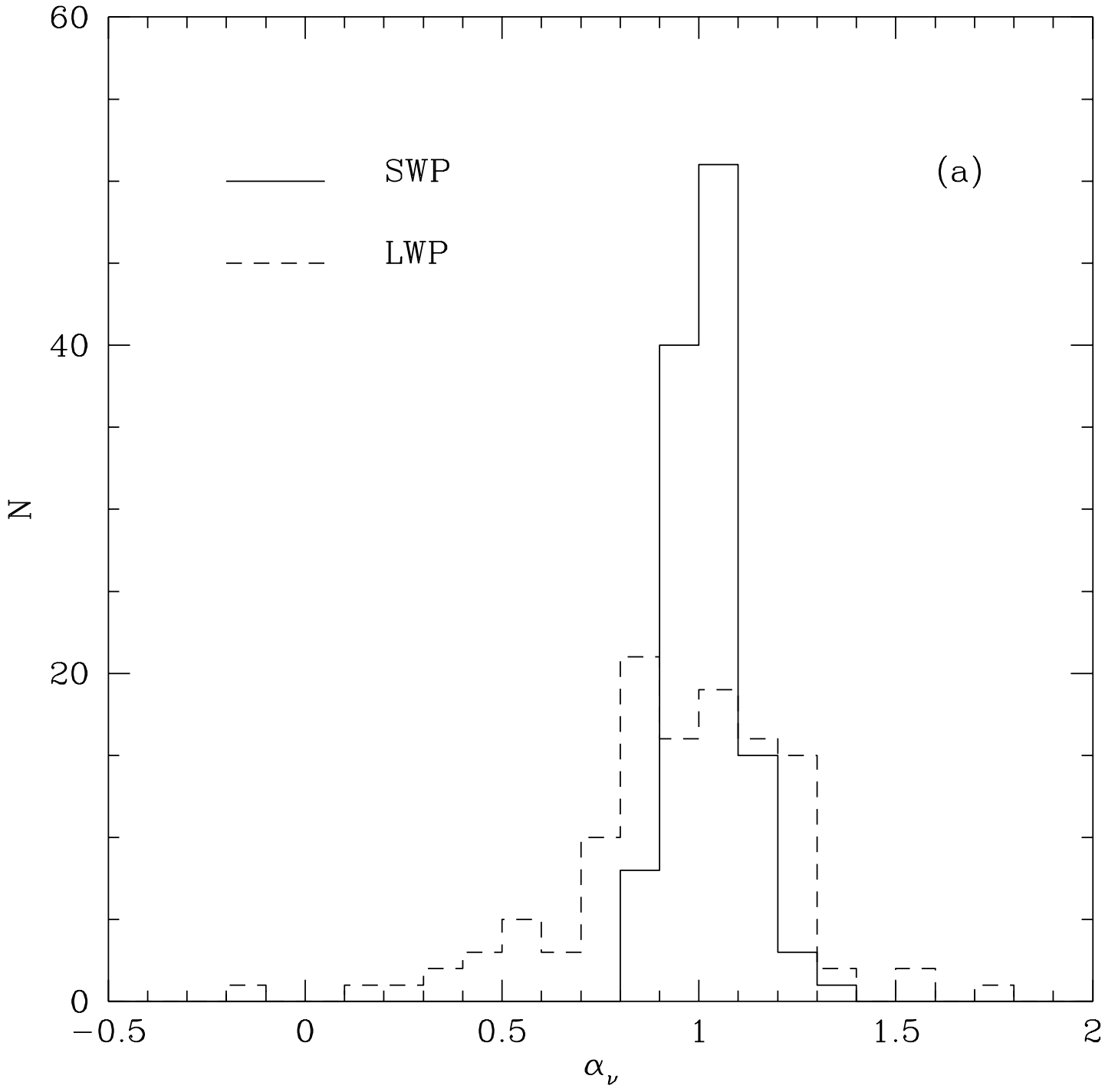
60
40
20
0
N
SWP
LWP
(a)
−0.5
0
0.5
1
1.5
2
α_ν

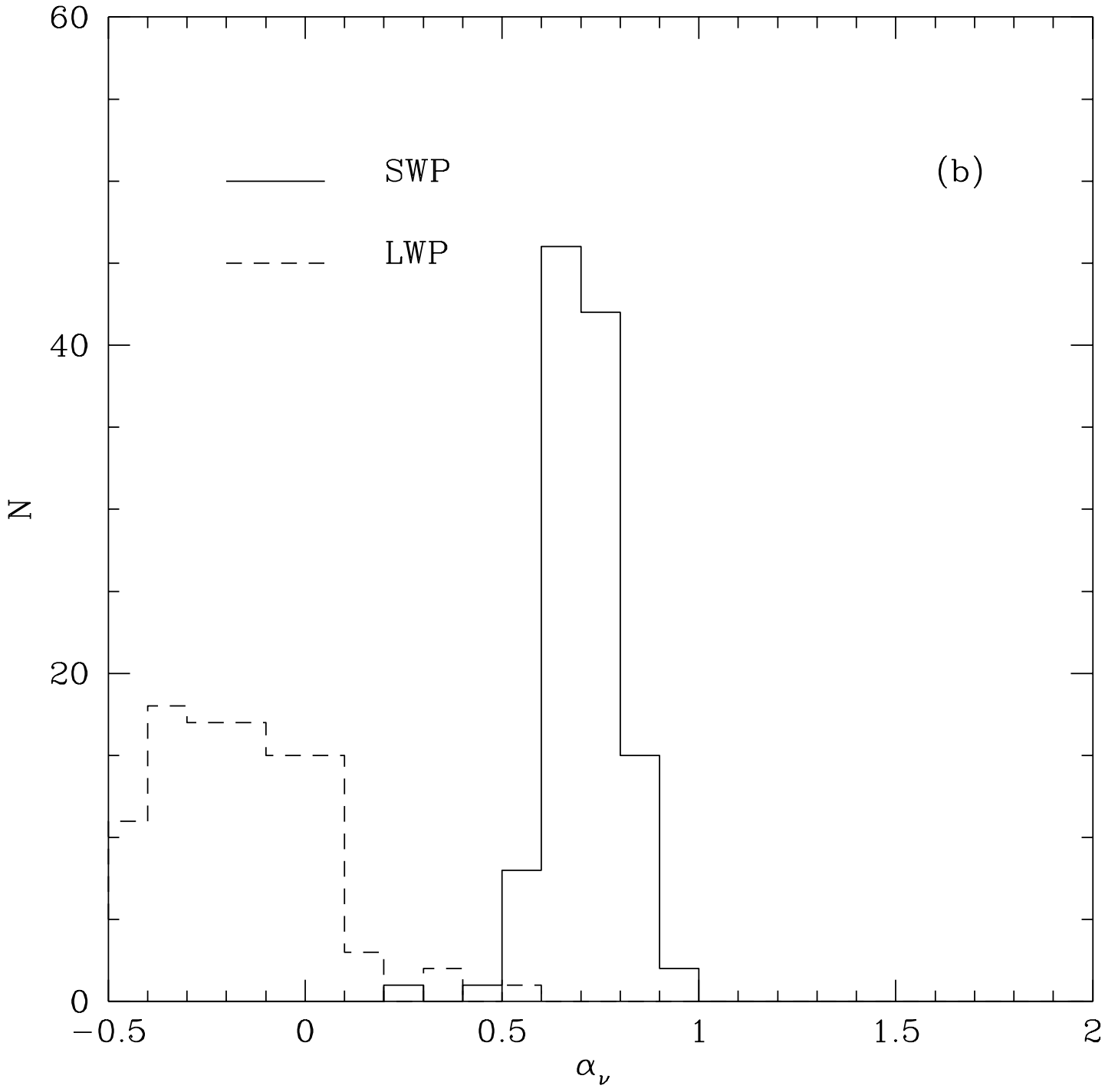
60
40
20
0
N
SWP
LWP
(b)
−0.5
0
0.5
1
1.5
2
α_ν

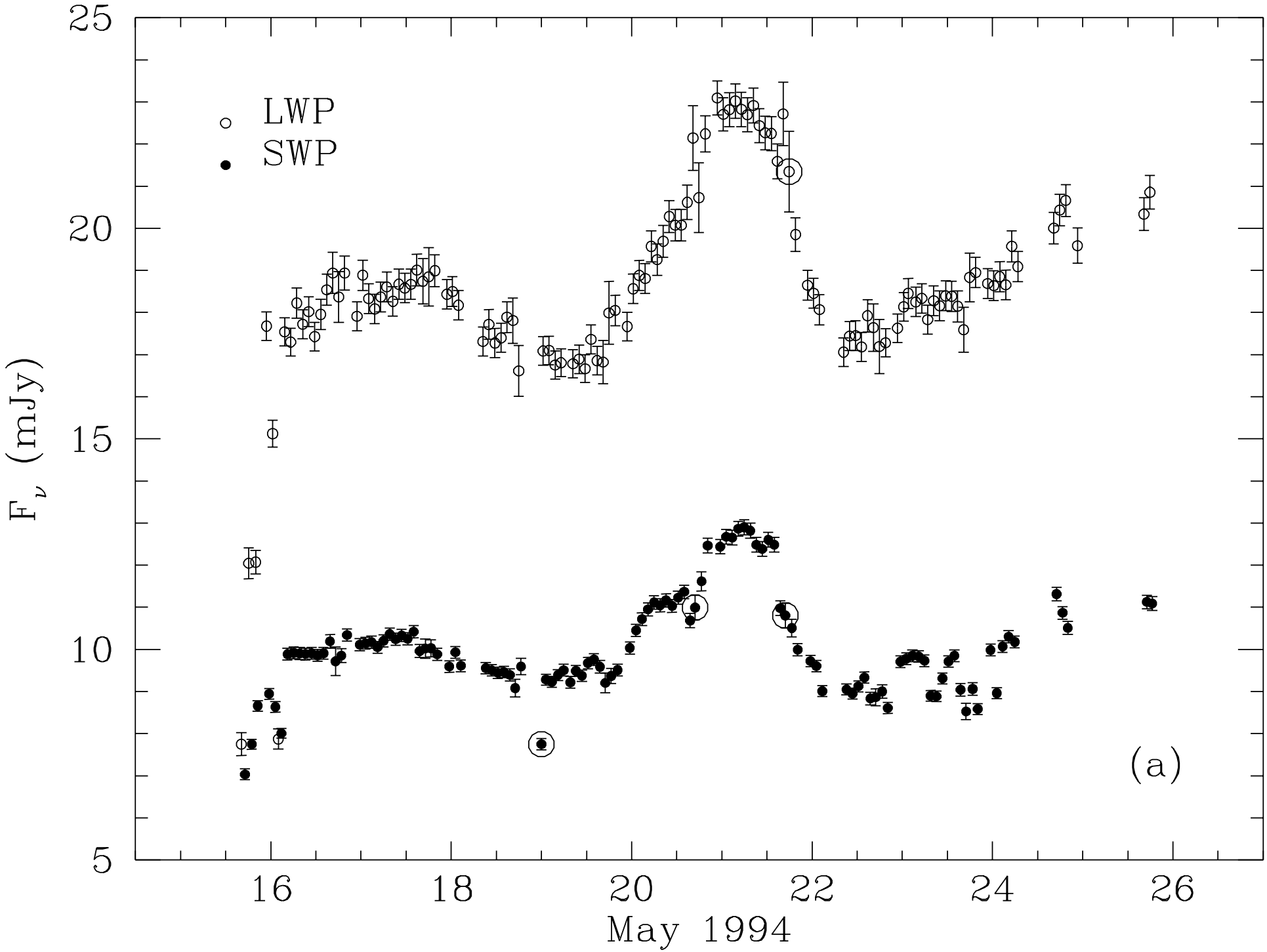
LWP
SWP
F_ν (mJy)
25
20
15
10
5
16
18
20
22
24
26
May 1994
(a)

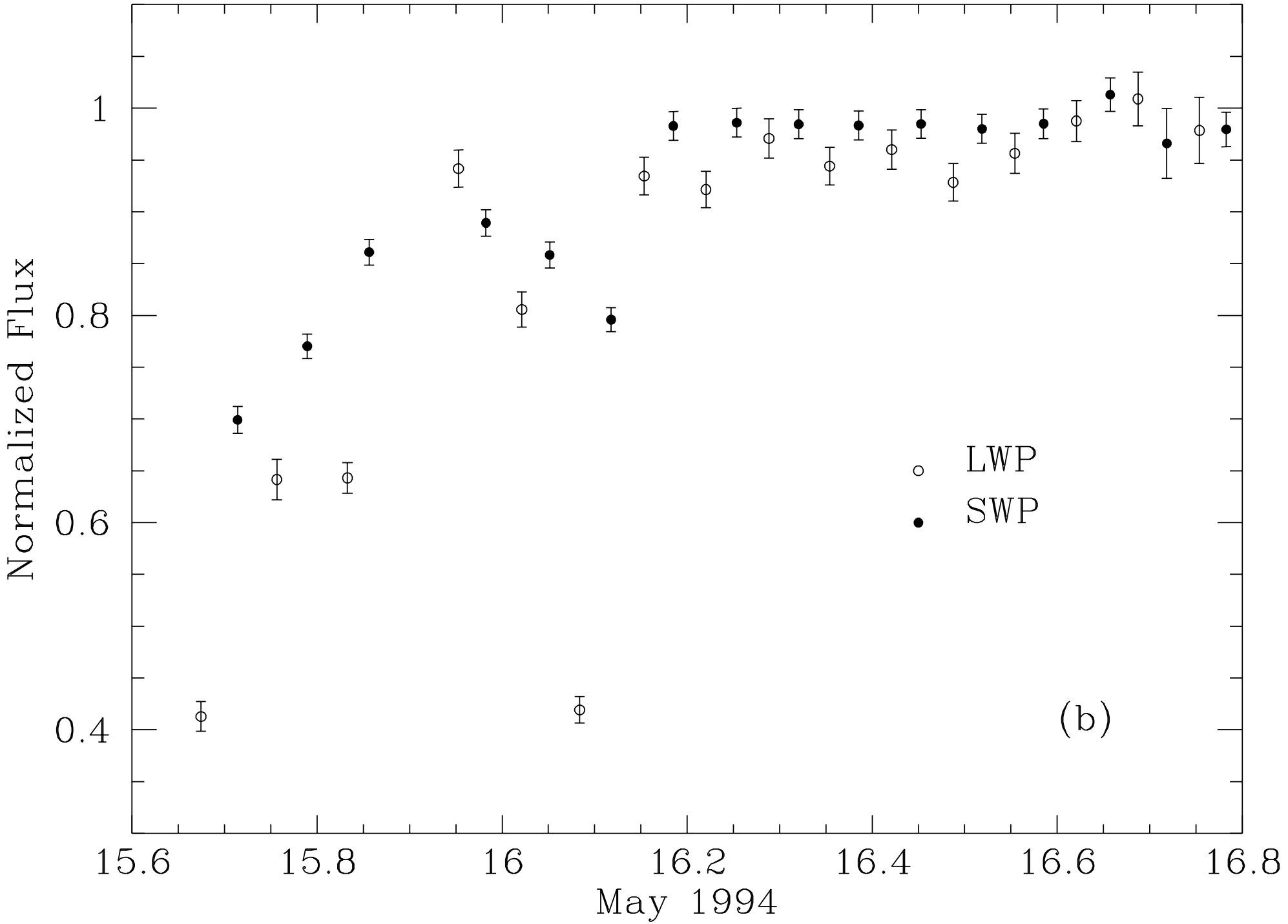
Normalized Flux
1
0.8
0.6
0.4
15.6
15.8
16
16.2
16.4
16.6
16.8
May 1994
LWP
SWP
(b)

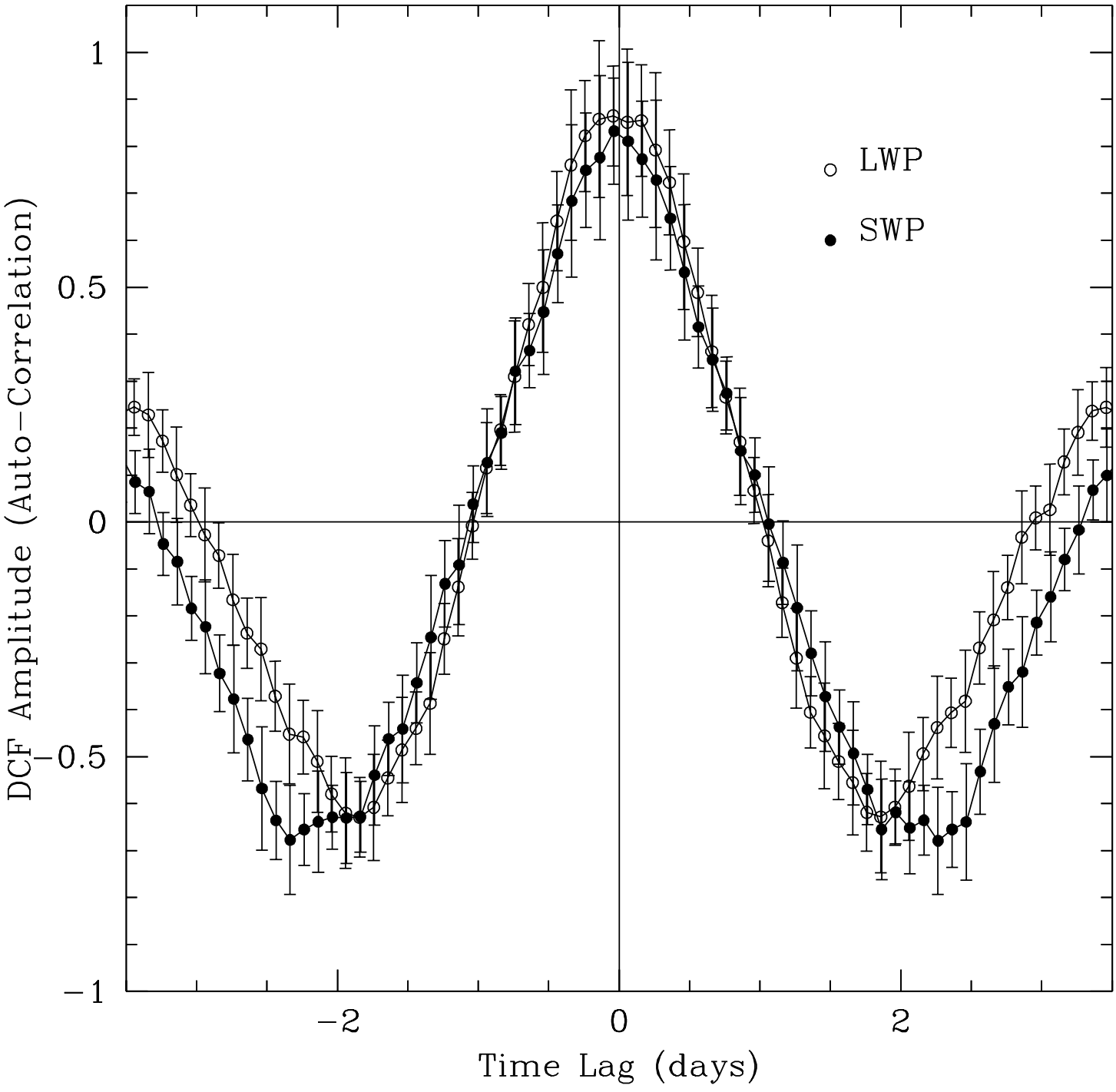
LWP
SWP
DCF Amplitude (Auto−Correlation)
Time Lag (days)
1
0.5
0
−0.5
−1
−2
0
2

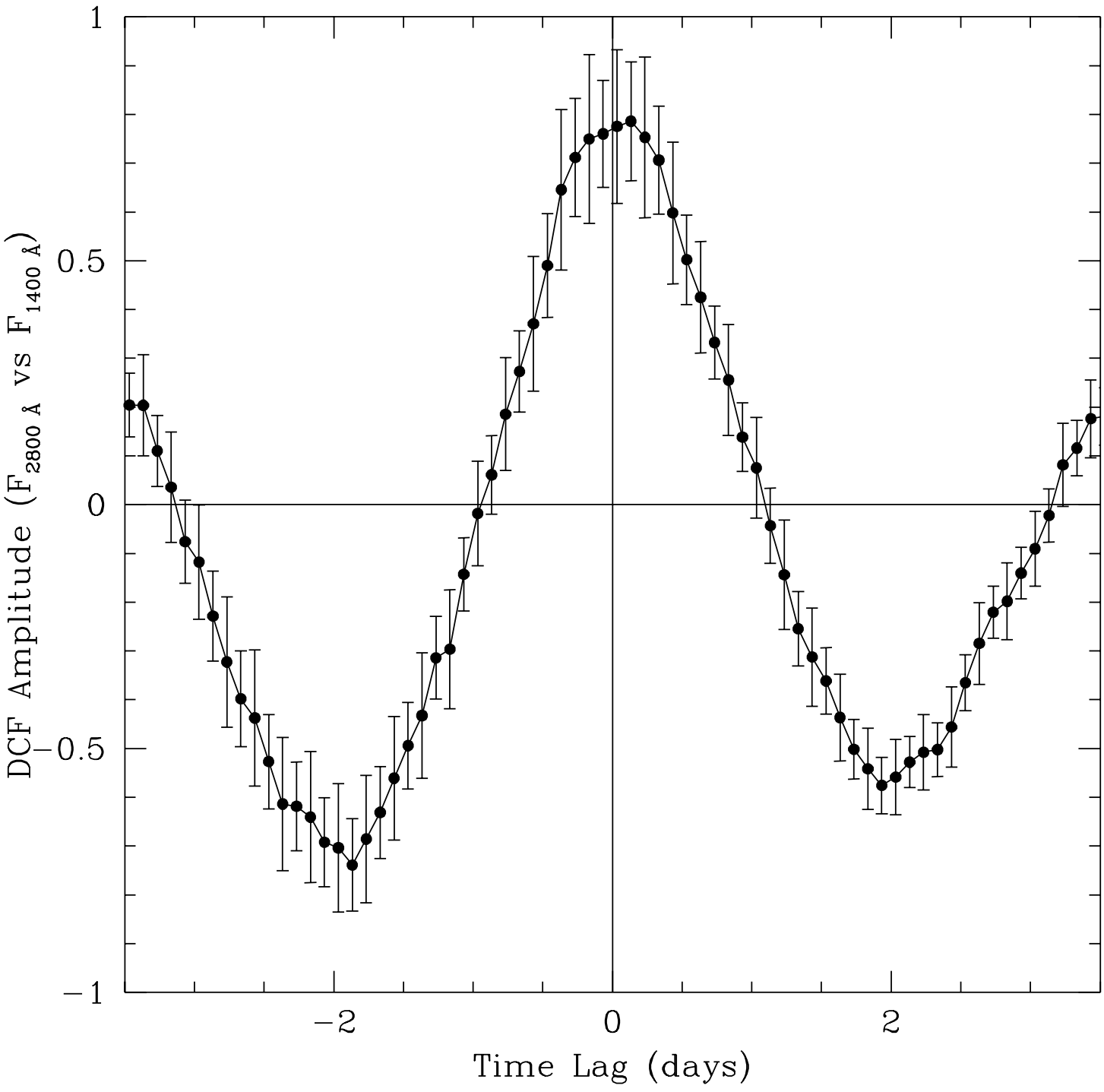
1
0.5
0
−0.5
−1
−2
0
2
DCF Amplitude ($F_{2800\ Å}$ vs $F_{1400\ Å}$)
Time Lag (days)

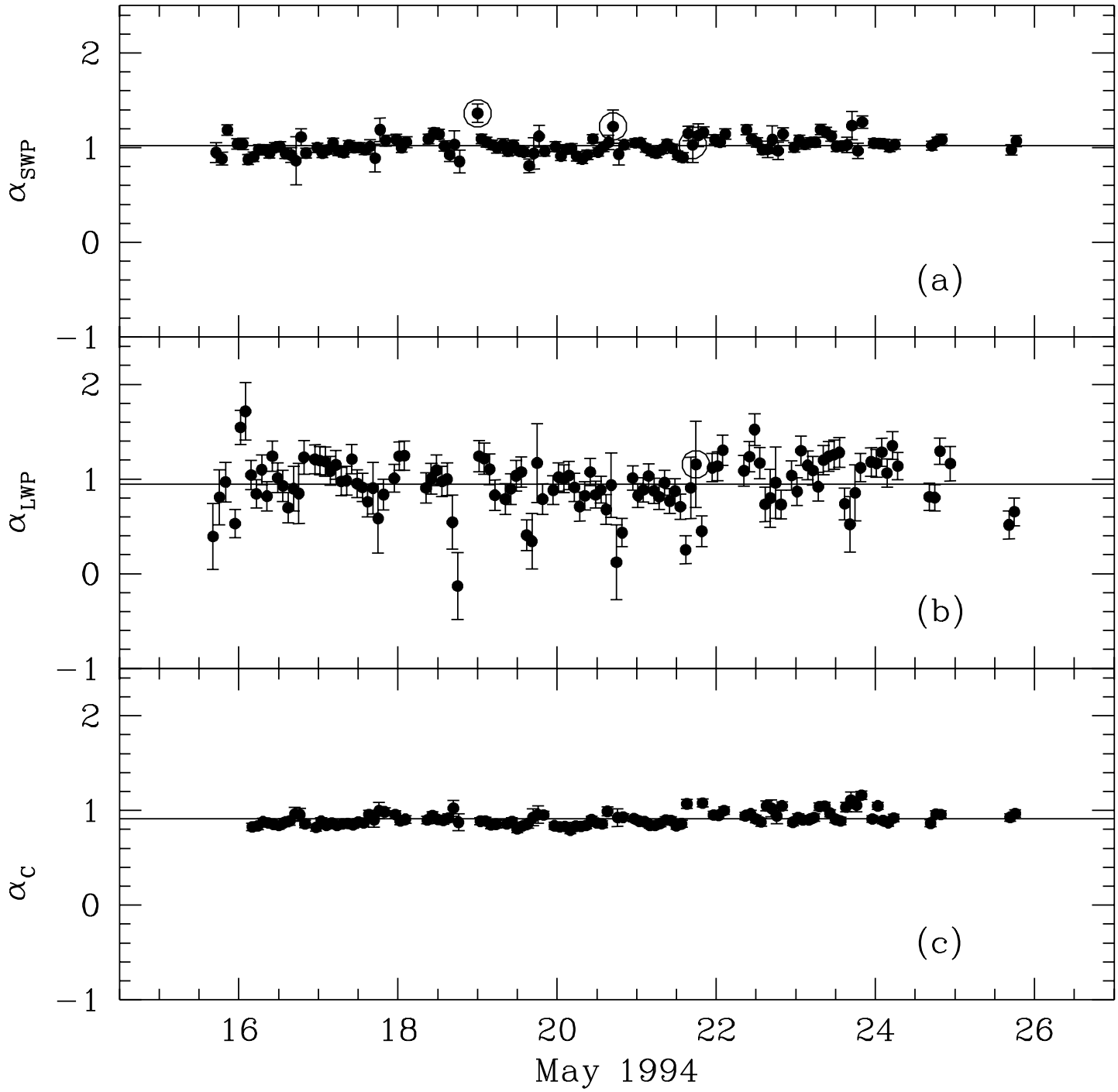
2
1
0
−1
α_{SWP}
(a)
2
1
0
−1
α_{LWP}
(b)
2
1
0
−1
α_c
(c)
16
18
20
22
24
26
May 1994

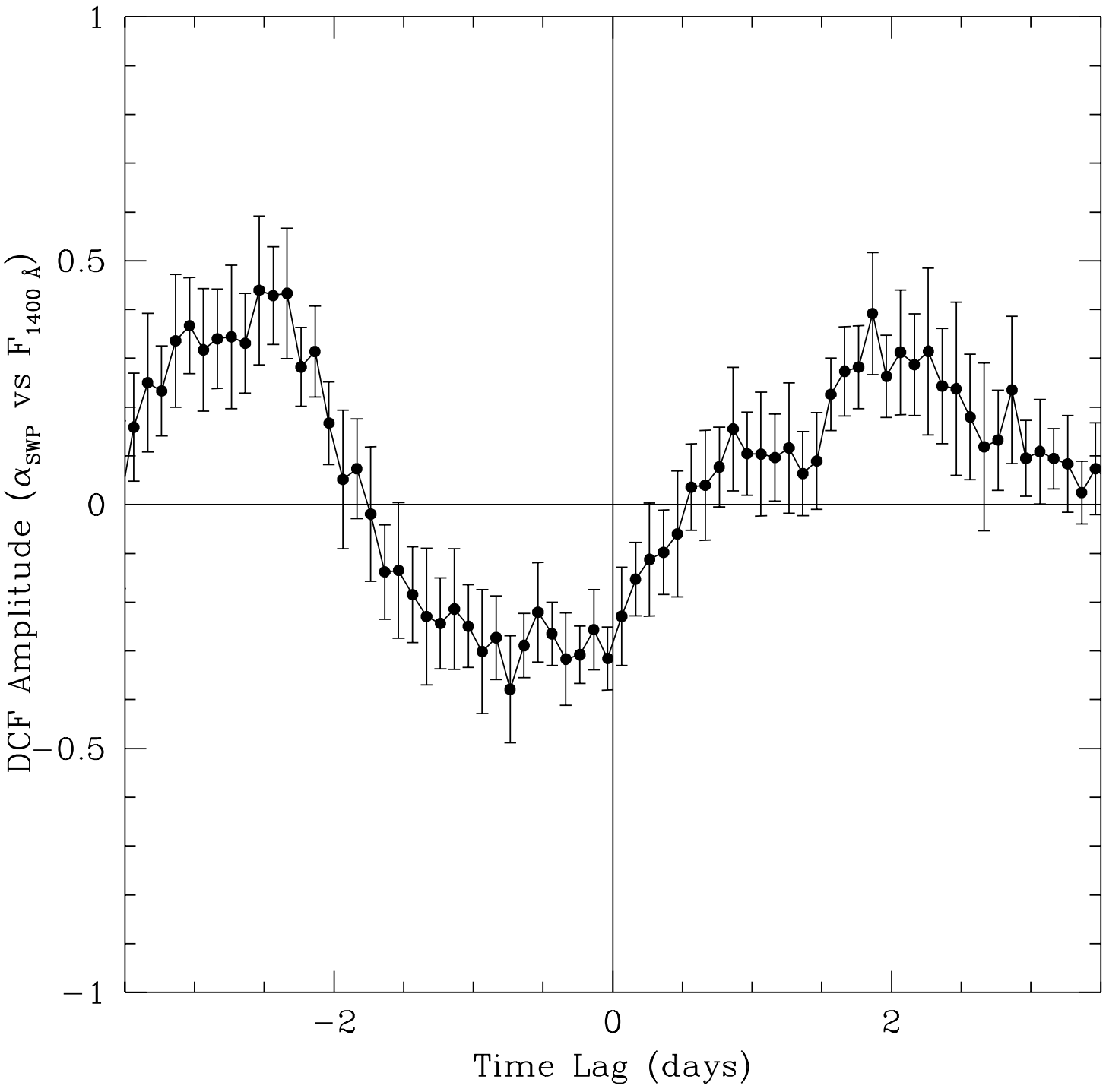
1
0.5
0
−0.5
−1
−2
0
2
DCF Amplitude (α_{SWP} vs $F_{1400\,Å}$)
Time Lag (days)

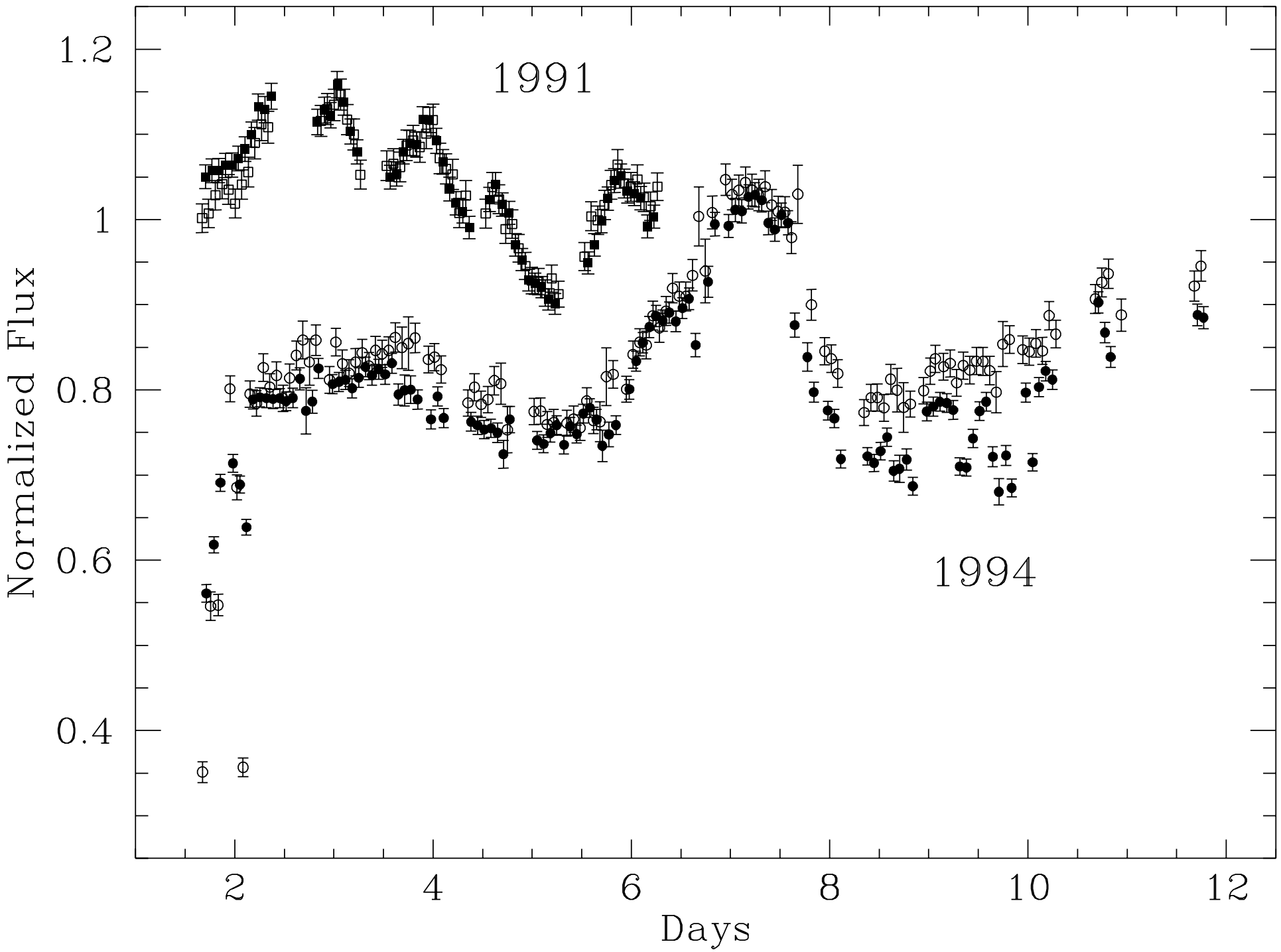
1991
1994
Normalized Flux
Days
1.2
1
0.8
0.6
0.4
2
4
6
8
10
12